All-Optical Logic Circuits based on the Polarization Properties of Non-Degenerate Four-Wave Mixing

Thesis by
Ashish Ishwar Singh Bhardwaj

In Partial Fulfillment of the Requirements
For the Degree of
Doctor of Philosophy

California Institute of Technology
Pasadena, California

2001
(Defended May 18, 2001)

To my parents

Acknowledgements

I would like to express my gratitude to my advisor, Professor Kerry Vahala for giving me the opportunity to be a member of his research group. I am indebted to him for the knowledge I have gained in the areas of Photonics and Quantum Electronics during my five years at Caltech.

I am extremely grateful to Prof. Vincent McKoy for his constant encouragement and support. He has rekindled my passion for science and I will forever remain indebted to him for being my mentor and for taking an active interest in the progress of my thesis. I am also very grateful to Dr. Per Olof Hedekvist for teaching me the skills required to be a good experimental scientist. Learning and working with him has been one of the most enriching and fruitful experiences of my life.

I am grateful to my friends Nathan Good and Dane Boysen for their friendship and moral support. I have shared many enlightening and fruitful discussions with them. I would like to acknowledge the following members of the Vahala group for making my stay at Caltech more enjoyable, Dr. David Geraghty, Dr. Dave Dougherty, Dr. Roberto Paiella, Dr. Mark Brongermsa, Sean Spillane, and Tobias Kippenberg. I would also like to thank Henrik Andersson, who is presently at Chalmers University of Technology in Sweden, for his help with my experiments. I would like to thank the following members of the Caltech staff, Jana Mercado, Linda Dosza, Greg Dunn, Lena Lenore, and Rosalie Rowe for their help with administrative matters.

I would like to thank the Division of Applied Physics and the Division of Chemistry for supporting my graduate studies in the form of teaching assistantships for three and a half years. I would like to acknowledge the National Science Foundation for its support in the form of a research assistantship for the last one and a half year.

My deepest thanks, of course, go to my parents for their unconditional support, patience and encouragement. Their love and understanding have helped me overcome the frustrations of graduate school.

Abstract

This thesis investigates a new class of all-optical logic circuits that are based on the polarization properties of non-degenerate Four-Wave Mixing. Such circuits would be used in conjunction with a data modulation format where the information is coded on the states of polarization of the electric field. Schemes to perform multiple triple-product logic functions are discussed and it is shown that higher-level Boolean operations involving several bits can be implemented without resorting to the standard 2-input gates that are based on some form of switching. Instead, an entire hierarchy of more complex Boolean functions can be derived based on the selection rules of multi-photon scattering processes that can form a new classes of primitive building blocks for digital circuits.

Possible applications of these circuits could involve some front-end signal processing to be performed all-optically in shared computer back-planes. As a simple illustration of this idea, a circuit performing error correction on a (3,1) Hamming Code is demonstrated. Error-free performance (Bit Error Rate of $< 10^{-9}$) at 2.5 Gbit/s is achieved after single-error correction on the Hamming word with 50 percent errors. The bit-rate is only limited by the bandwidth of available resources. Since Four-Wave Mixing is an ultrafast nonlinearity, these circuits offer the potential of computing at several terabits per second. Furthermore, it is shown that several Boolean functions can be performed in parallel in the same set of devices using different multi-photon scattering processes. The

main objective of this thesis is to motivate a new paradigm of thought in digital circuit design. Challenges pertaining to the feasibility of these ideas are discussed.

Contents

List of Figures

Chapter 1

Introduction

1.1 Background

Data transmission speeds over fiber optic networks have been steadily increasing over the past decade. Commercial systems capable of transmitting hundreds of gigabits per second are available and systems demonstrations of over a terabit per second (one terabit is 10^{12} bits) transmission have been demonstrated experimentally [1-4]. Record transmission rates of over 10 terabits per second have been recently demonstrated [5, 6]. Long-haul transmission over thousands of kilometers is made possible with the availability of extremely low loss optical fibers (typically 0.2 dB/km) and the invention of the Erbium-Doped Fiber Amplifiers (EDFAs) [7]. Thus it is now possible to develop high capacity long-haul photonic networks and this is an active field of research in many leading organizations across the world [8-12]. As the aggregate data rates increase, the efficiency of the photonic network is limited by the speed of the electronics at the transmitters and receivers in the network. Similar limitations are imposed by the presence of electronic switches and routers. This is frequently referred to as the "electronic bottleneck" that has led to an increased interest in trying to develop techniques to add optical functionality to

enable signal processing to be accomplished in the all-optical domain. Nonlinear optics has been studied extensively to develop techniques to enable different forms of signal processing in the optical domain and some of the techniques are reviewed in this thesis. A third-order nonlinear process, namely Four-Wave Mixing (FWM) is studied in greater detail. Applications of FWM for ultrafast optical logic are reviewed and a new class of all-optical logic gates using the polarization properties of FWM is proposed and demonstrated [13-16].

1.2 Thesis Outline

A review of optical switching technologies based on nonlinear effects is presented in Chapter 2. FWM in Semiconductor Optical Amplifiers (SOA) is discussed in Chapter 3 and pertinent issues such as the device length and dependence of FWM on the polarization of the electric fields involved are reviewed. The concepts of a Spectral Data Bus and Polarization Shift Keying (PolSK) as new modes of data transmission on an optical fiber are discussed in Chapter 4. This sets the premise to consider the feasibility of using the polarization dependence of the FWM process to develop a new class of optical logic gates. Keeping simple front-end applications on a spectral data bus in mind, on-the-fly error detection and correction on a spectral bus is considered in detail and an Error Detecting and Correcting circuit for a (3,1) Hamming Code based on the polarization properties of FWM is proposed. Details of the construction of this circuit along with the results obtained on its successful demonstration are presented in Chapter 5. The ideas

proposed for the (3,1) Hamming Code are further generalized in Chapter 6 where the scheme is extended to implement a full 3-bit adder. New circuit designs based on the 3-bit adder as fundamental building blocks for other higher level Hamming Codes, such as the (7,4) Code are proposed.

Bibliography

1. T.N. Nielsen, A.J. Stentz, K. Rottwitt, D.S. Vengsarkar, Z.J. Chen, P.B. Hansen, J.H. Park, K.S. Feder, S. Cabot, S. Stulz, D.W. Peckham, L. Hsu, C.K. Kan, A.F. Judy, S.Y. Park, L.E. Nelson, and L. Gruner-Nielsen, "3.28 Tb/s Transmission over 3 x 100 km of Nonzero-Dispersion Fiber using Dual C- and L-band Distributed Raman Amplification," *IEEE Photonic. Tech. Lett.,* **12**, 1079-1081 (2000).

2. A.R. Chraplyvy, "High-Capacity Lightwave Transmission Experiments," *Bell Labs Tech. J.,* **4**, 230-245 (1999).

3. A.R. Chraplyvy, A.H. Gnauck, R.W. Tkach, J.L. Zyskind, J.W. Sulhoff, A.J. Lucero, Y. Sun, R.M. Jopson, F. Forghieri, R.M. Derosier, C. Wolf, and A.R. McCormick, "1-Tb/s Transmission Experiment," *IEEE Photonic. Tech. Lett.,* **8**, 1264-1266 (1996).

4. Y. Yambayashi and M. Nakazawa, "Terabit Transmission Technology," *NTT Review*, **11**, 23-32 (1999).

5. K. Fukuchi, T. Kasamatsu, M. Morie, R. Ohhira, T. Ito, K. Sekiya, D. Ogasahara, and T. Ono, "10.92 Tb/s (273 x 40-Gb/s) Triple-Band/Ultra-Dense WDM Optical-Repeatered Transmission Experiment," Post-deadline paper, PD-24, *OFC' 2001,* Anaheim, CA, March 17-22 (2001).

6. S. Bigo,Y. Frignac, G. Charlet, S. Borne, P. Tran. C. Simonneau, D. Bayart, A. Jourdan, J.P. Hamaide, W. Idler, R. Dischler, G. Veith, H. Gross, and W. Poehlmann, "10.2 Tb/s (256 x 42.7 Gbit/s PDM/WDM) Transmission Over 100 km TeraLight^{TM} Fiber with 1.28 Bit/s/Hz Spectral Efficiency," Post-deadline paper , PD-25, *OFC' 2001,* Anaheim, CA, March 17-22 (2001).

7. R.J. Mears, L. Reekie, I.M. Jauncey, and D.N. Payne, "Low Noise Erbium-Doped Fiber Amplifier Operating at 1.54 μm," *Electron. Lett.,* **23**, 1026-1028 (1987).

8. D.K. Hunter, and I. Andonovic, "Approaches to Optical Internet Packet-Switching," *IEEE Commun. Mag.,* **38**, 116-122 (2000).

9. S. Yao, B. Mukherjee, and S. Dixit, "Advances in Photonic Packet Switching: An Overview," *IEEE Commun. Mag.,* **38**, 84-94 (2000).

10. R. S. Tucker, and W. De Zhong, "Photonic Packet Switching: An Overview," *IEICE T. Electron.,* **E82C**, 202-212 (1999).

11. C. Guillemot, M. Renaud, P. Gambini, C. Janz, I. Andonovic, R. Bauknecht, B. Bostica, M. Burzio, F. Callegati, M. Casoni, D. Chiaroni, F. Clerot, S.L. Danielsen, F. Dorgeuille, A. Dupas, A. Franzen, P.B. Hansen, D.K. Hunter, A. Kloch, R. Krahenbuhl, B. Lavigne, A. Le Corre, C. Raffaelli, M. Schilling, J.C. Simon, and L. Zucchelli, "Transparent Optical Packet Switching: The European ACTS KEOPS Project Approach," *J. Lightwave Technol.,* **16**, 2065-2067 (1998).

12. V.W.S. Chan, K.L. Hall, E. Modiano, and K.A. Rauschenbach, "Architectures and Technologies for High-Speed Optical Data Networks," *J. Lightwave Technol.,* **16**, 2146-2168 (1998).

13. A. Bhardwaj, P.O. Hedekvist, and K. Vahala, "All-Optical Logic Circuits Based on Polarization Properties of Nondegenerate Four-Wave Mixing," *J. Opt. Soc. Am. B*, **18**, 657-665 (2001).

14. P.O. Hedekvist, A. Bhardwaj, K. Vahala, and H. Andersson, "Advanced All-Optical Logic Gates on a Spectral Bus," *Appl. Opt.,* **40**, 1761-1766 (2001).

15. P.O. Hedekvist, A. Bhardwaj, K. Vahala, and H. Andersson, "Multiple-Input All-Optical Logic Gates Utilizing Polarization Properties of Non-Degenerate Four-Wave

Mixing," Paper UFB2, presented at the *Topical Meeting on Ultrafast Electronics and Optoelectronics*, Lake Tahoe, Nevada, Jan. 10-12 (2001).

16. A. Bhardwaj, P.O. Hedekvist, H. Andersson, and K.J. Vahala, "All Optical Front End Error Correction on a Spectral Data Bus," Paper CWI5, presented at the *Conference on Lasers and Electro-Optics*, San Francisco, CA, May 7-12 (2000).

Chapter 2

Applications of Nonlinear Optics in High-Speed Digital Processing

---

2.1 Introduction

Nonlinear optics has been of increased interest for all-optical signal processing in high-speed photonic networks [1, 2]. Sample applications include all-optical switching as well as demultiplexing [3-5]. In addition, Boolean operations such as Exclusive-OR (XOR) and 2-bit addition have been demonstrated optically using a combination of such switching devices [6, 7]. Devices have employed both fiber-based and semiconductor-based nonlinear elements. In the former case, the physical nonlinearity is the Kerr nonlinearity of silica glass. In the latter case, the nonlinearity results from a variety of ultrafast mechanisms in semiconductor gain media, including carrier heating and spectral hole burning [8]. Apart from long-haul data transmission, all-optical logic gates might someday find applications in local area networks to provide certain limited all-optical functionality. Such functions will only make sense where equivalent electrical solutions are cumbersome or when a real advantage can be realized by maintaining signals in

optical form. In Wavelength Division Multiplexed (WDM) systems there has been interest in all-optical functionality for switching and routing, but so far very limited implementation of these functions [9, 10]. The likelihood of more sophisticated all-optical functions will be higher should Time Division Multiplexed (TDM) or mixed TDM/WDM systems be implemented since this format lends itself better to a variety of well-established all-optical switching solutions [1].

2.2 Switching Based on Cross-Phase Modulation

Optical switching using a nonlinear interferometer makes it possible for one optical signal to control and switch another optical signal through the nonlinear interaction in a material. The input signal to be switched is split between the arms of the interferometer. The interferometer is balanced so that, in the absence of a control signal, the input signal emerges from one output port. The presence of a strong control pulse changes the refractive index of the medium given by

$$\Delta n = n_2 I, \tag{2-1}$$

where Δn is the change in the refractive index of the medium, n_2 is the nonlinear refraction coefficient and I is the intensity of light incident on the medium. A change in the index adds a phase shift between the two arms of the interferometer, so that the input

signal is switched over to a second output port. This method of switching based on cross-phase modulation (XPM) is schematically shown in Figure 2.1.

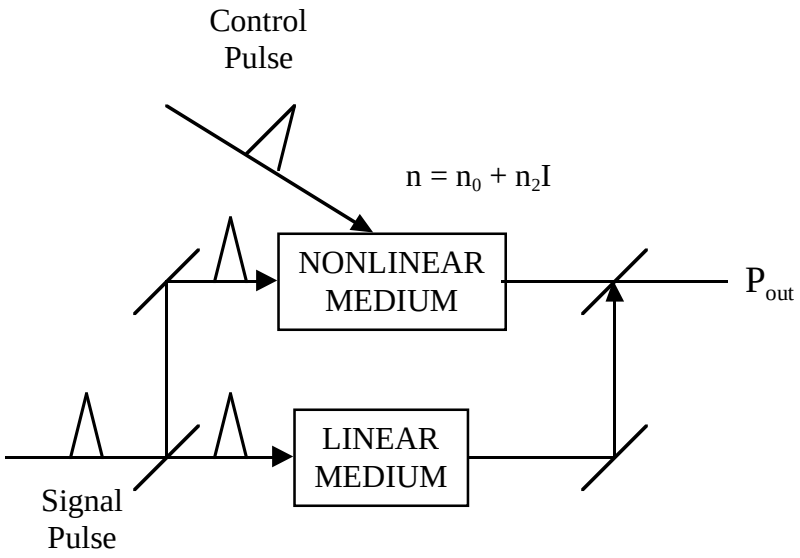

Figure 2.1: All-optical switching using XPM in a nonlinear interferometer

A. The Nonlinear Optical Loop Mirror (NOLM)

One way to implement XPM-based switching is to use a Sagnac interferometer, where one of the output ports also serves as the input port for the signal to be switched. This configuration is commonly referred to as the Nonlinear Optical Loop Mirror (NOLM) [11] and is shown in Figure 2.2.

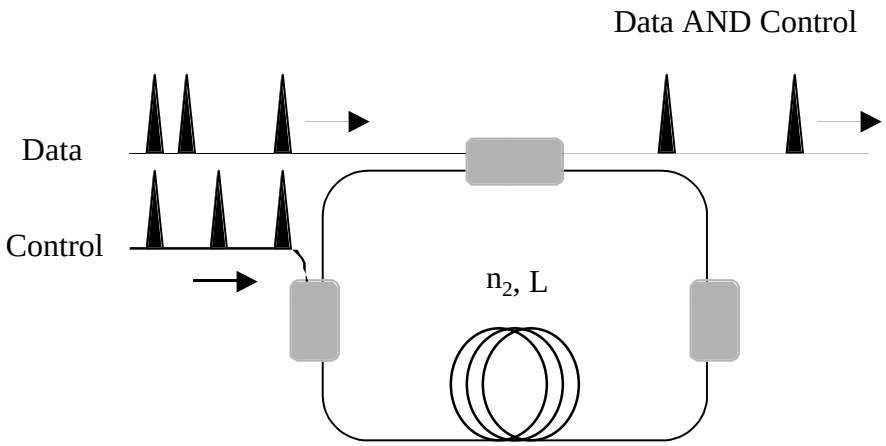

Figure 2.2: The Nonlinear Optical Loop Mirror (NOLM)

The input coupler splits the input signal pulse into two counter-propagating pulses, which subsequently combine again at the coupler, each having traveled around the loop. A strong control pulse is then introduced into the loop as a unidirectional beam. The nonlinear optical effect of the control pulse is to induce a refractive index change, Δn, which is experienced fully by a co-propagating signal pulse. This refractive index change results in a differential phase shift, $\Delta\emptyset$, between the counter-propagating signal pulses as they arrive back at the input coupler, given by

$$\Delta\emptyset = k\,\Delta n\,L, \tag{2-2}$$

where k is the wavevector and L is the path length over which the induced index change Δn is effective. The path length is chosen such that complete switching occurs, i.e., the

phase shift is π radians. In a fiber interferometer, the physical mechanism is the intrinsic Kerr nonlinearity of glass [12]. Since the optical nonlinearity in glass is very small ($n_2 \approx 3\times10^{-20}$ m^2 W^{-1} for silica), a device control power-length product of typically ~1 W-km is needed for a phase shift of π. In practice, fiber interferometer path lengths of several kilometers are needed to keep the average control power to below 100 mW. The long path lengths make it difficult to build stable and compact devices.

B. The Terahertz Optical Asymmetric Demultiplexer (TOAD)

A Semiconductor Optical Amplifier (SOA) is similar to a semiconductor laser diode, except that the reflectivity of the end faces is deliberately minimized to suppress lasing. Thus the SOA acts as a one-pass device for a lightwave with an inversion that is created by electrical pumping. The conduction and valence bands in a semiconductor can be modeled as an ensemble of two level atom-like systems, which are coupled through various scattering mechanisms. These scattering mechanisms which control the evolution of the two-level systems will be discussed in greater detail in Chapter 3. For photons that are resonant with the transition energy levels of the states that are inverted, stimulated emission can occur, i.e., photons at these frequencies see a gain. As the intensity of light increases, the gain saturates from the depopulation of the conduction band due to stimulated emission. Associated with this change in the gain due to saturation is a refractive index change, as described by the Kramer-Krönig dispersion relations. The refractive nonlinearity of the SOA is ~10^8 times larger than an equivalent length of silica

fiber. The relaxation time associated with the relaxation of the refractive index to its equilibrium value is governed by the interband carrier lifetime, and is typically 100-500 picoseconds.

Since the interband carrier lifetimes are very slow, switching at data-rates much higher than 1 Gbit/s based on inter-band carrier relaxation did not seem possible. This limitation was overcome by placing the SOA asymmetrically with respect to the center of the loop in the Sagnac interferometer, as shown in Figure 2.3. This is called the Semiconductor Laser Amplifier in a Loop Mirror (SLALOM) [13] or Terahertz Optical Asymmetric Demultiplexer (TOAD) [14]. Since the rise time associated with the change in refractive index is less than a picosecond [15], it is possible to obtain a switching window which is shorter than the recovery time limited by the inter-band carrier relaxation. It has been demonstrated that a window width of ≤ 10 picoseconds can be created which allows demultiplexing a 50 GHz pulse train down to a base rate of 1 GHz [16]. By operating the SOA in strong saturation, the carrier relaxation time can be modified to ~25 picoseconds [17]. The XPM bandwidth also increases with the device length due to traveling wave effects [18, 19] and demonstrations of wavelength conversion at 100 Gbit/s using XPM have been reported [20].

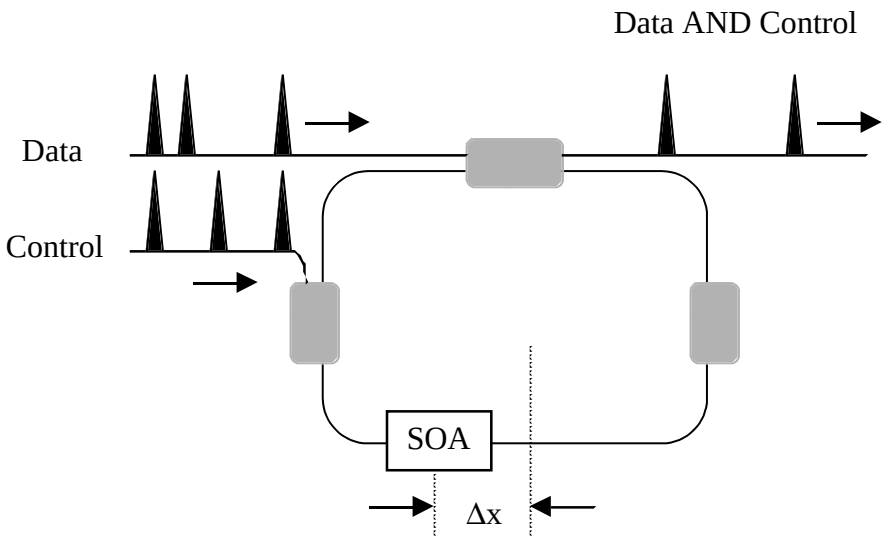

Figure 2.3: The Terahertz Optical Asymmetric Demultiplexer (TOAD)

There have been successful demonstrations of different optical functionalities using configurations based on the NOLM and TOAD. These include demultiplexers [3, 17] and the implementation of simple Boolean functions such as AND, NOT and Exclusive-OR (XOR) for address recognition [21, 22]. More sophisticated Boolean functions such as 3-bit adders [23, 24] and parity bit generators [25] have been demonstrated using a combination of several TOAD-based gates.

C. The Ultrafast Nonlinear Interferometer (UNI)

The UNI is a balanced, single-arm interferometer that does not require any external stabilization of the interferometer arms. The signal pulse that is to be switched is split into two orthogonal polarization components with a time delay (typically equal to half the bit period) by passing it through highly birefringent fiber. The two orthogonal pulses then pass through a SOA and are temporally recombined after passing through a second birefringent fiber and interfered. The State of Polarization of the signal pulse after recombining is determined by the induced phase changes from the time-dependent refractive index changes in the presence of a control pulse (which could be co-propagating or counter-propagating) that is aligned temporally with one of the orthogonal pulses in the SOA. The signal pulse then passes through a fiber polarizer that is adjusted such that the signal pulse is orthogonal to the polarizer in the presence of the control pulse and parallel to the polarizer when the control pulse is not present. 100 Gbit/s bit-wise switching has been demonstrated using the UNI gate [10]. A schematic of the UNI gate is shown in Figure 2.4.

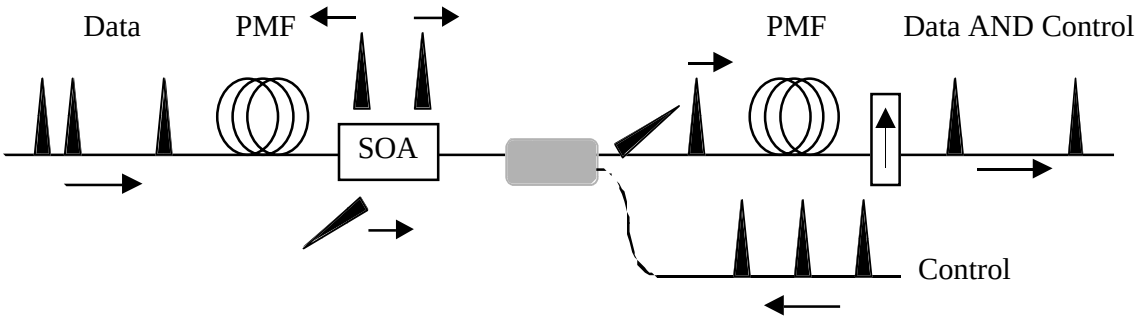

Figure 2.4: The Ultrafast Nonlinear Interferometer (UNI)

For dual rail logic, such as XOR, the phase of each polarization state can be accessed and changed independently by two separate control pulses. All-optical XOR gate based on the UNI has been demonstrated on a 40 GHz clock pulse [26] and at 20 Gbit/s [27]. A 40 GHz all-optical shift-register with an inverter has also been demonstrated using 2 mm SOAs in the UNI gate configuration [28].

Other important applications of XPM in advanced optical communications systems include regeneration and wavelength conversion in the optical domain. Regeneration is essential to remove the errors at the detection-end caused by the distortion of the signal due to noise, dispersion, and crosstalk. This is called 3R regeneration, where the signal is reamplified, reshaped and retimed [13]. 3R regeneration along with wavelength conversion at 80 Gbit/s with error-free operation has been demonstrated using XPM in a nonlinear Mach-Zehnder Interferometer (MZI) with a SOA [29]. Interferometric gates based on XPM in SOAs using the Mach-Zehnder or Michaelson configuration have been integrated on planar lightwave circuits and are reviewed in [30]. Figure 2.5 shows a schematic of a Mach-Zehnder Interferometer (MZI) gate to obtain a short switching window by adding a time delay between the control pulses entering each arm of the interferometer.

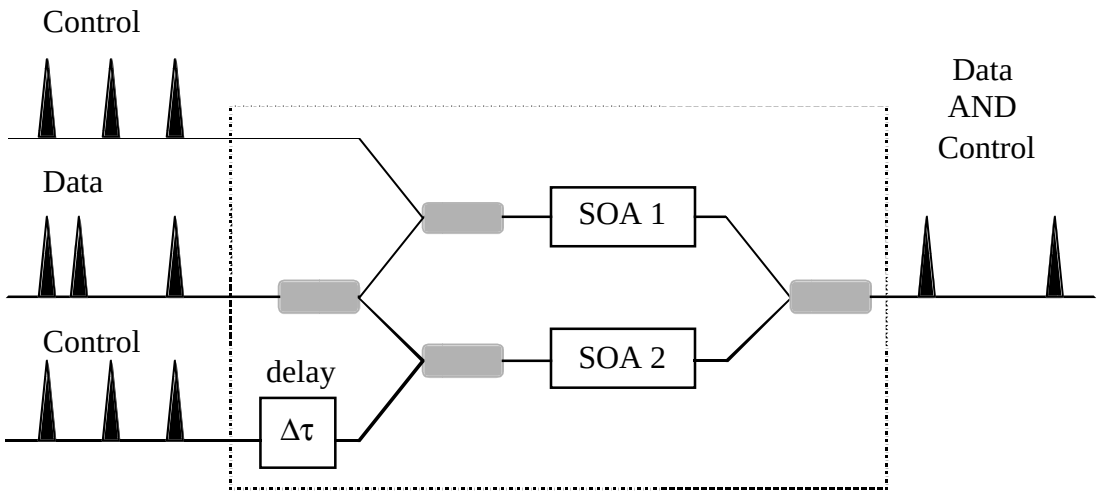

Figure 2.5: Schematic of the Mach-Zehnder Interferometer (MZI) gate that uses a time delay between the control pulses entering each arm to open a small switching window

2.3 Switching Based on Cross-Gain Modulation

The Cross-Gain Modulation (XGM) uses an input signal to saturate the gain and thereby modulate a Continuous Wave (CW) signal at a desired output wavelength. Wavelength conversion at 100 Gbit/s using XGM in SOAs has been demonstrated [31]. Although simple to implement, the XGM gate has a number of shortcomings, such as inversion of the input-control signal and the relatively large chirp of the output signal due to the large gain modulation. Format conversion from Return to Zero (RZ) to Non-Return to Zero (NRZ) and vice versa has been demonstrated using XGM gates [32].

2.4 Ultrafast Switching Based on Four-Wave Mixing

The TOAD based gates are limited by the interband carrier lifetimes. Higher speeds of operation can be obtained in SOAs by nonlinear processes that involve intraband transitions, such as Four-Wave Mixing (FWM). FWM in active semiconductor gain media will be investigated in more detail in Chapter 3. In short, the intraband processes leading to FWM are carrier heating (CH) and spectral hole burning (SHB) [8]. The speed of CH process is limited by carrier-phonon scattering lifetime and SHB is limited by carrier-carrier scattering lifetime, i.e., the time required to establish a Fermi-Dirac distribution of the carrier population. These CH and SHB lifetimes have been measured experimentally by Zhou *et al.* [33] and it is believed that carrier-carrier scattering occurs at a time scale of 50-100 femtoseconds. Thus in principle, optical logic gates based on FWM in SOAs with speeds of a few terabits per second are possible. FWM in SOAs has been used for applications such as demultiplexing [34], wavelength conversion [34] and even dispersion compensation using optical phase conjugation [35]. All-optical AND gates have been developed and error-free performance at 100 Gbit/s has been demonstrated [36]. Applications of AND gates also include address recognition of optical packets [36] and clock-recovery [37].

As OTDM or mixed TDM/WDM systems evolve to higher levels of sophistication and speed, optical logic gates and circuits built using a combination of such gates will be used not only for demultiplexing, wavelength conversion and 2R/3R

regeneration, but also for header recognition for all-optical packet switched networks to enable all-optical routing, coding and decoding for error detection and correction and possibly encryption for added security. Though at present such devices cannot be as densely integrated on a chip as their electronic equivalents, they offer advantage in terms of speed and compatibility with state-of-the-art optical transmission systems. With the development of newer network architectures and protocols, all-optical logic gates will be used increasingly in tandem with electronics to greatly enhance the capacity and throughput of future communications networks.

Bibliography

1. D. Cotter, R.J. Manning, K.J. Blow, A.D. Ellis, A.E. Kelly, D. Nesset, I.D. Phillips, A.J. Poustie, and D.C. Rogers, "Nonlinear Optics for High-Speed Digital Information Processing," *Science*, **286**, 1523-1528 (1999).

2. V.W.S. Chan, K.L. Hall, E. Modiano, and K.A. Rauschenbach, "Architectures and Technologies for High-Speed Optical Data Networks," *J. Lightwave Technol.,* **16**, 2146-2168 (1998).

3. T. Yamamoto, E. Yoshida, and M. Nakazawa, "Ultrafast Nonlinear Optical Loop Mirror for Demultiplexing 640 Gbit/s TDM Signals," *Electron. Lett.,* **34**, 1013-1014 (1998).

4. K. Uchiyama, H. Takara, S. Kawanishi, T. Morioka, and M. Saruwatari, "Ultrafast Polarization-Independent All-Optical Switching Using a Polarization Diversity Scheme in the Nonlinear Optical Loop Mirror," *Electron. Lett.,* **28**, 1864-1866 (1992).

5. M. Eiselt, W. Pieper, and H.G. Weber, "All-optical High-Speed Demultiplexing with a Semiconductor-Laser Amplifier in a Loop Mirror Configuration," *Electron. Lett.,* **29**, 1167-1168 (1993).

6. A.J. Poustie, K.J. Blow, A.E. Kelly, and R.J. Manning, "All-Optical Binary Half-Adder," *Opt. Commun.,* **156**, 22-26 (1998).

7. R.J. Manning, A.D. Ellis, A.J. Poustie, and K.J. Blow, "Semiconductor Laser Amplifiers for Ultrafast All-Optical Signal Processing," *J. Opt. Soc. Am. B,* **14**, 3204-3216 (1997).

8. G.P. Agrawal, "Population Pulsation and Nondegenerate Four-Wave Mixing in Semiconductor Laser Amplifiers," *J. Opt. Soc. Am. B*, **5**, 147-159 (1988).

9. D. Nesset, M.C. Tatham, L.D. Westbrook, and D. Cotter, "Degenerate Wavelength Operation of an Ultrafast All-Optical AND Gate Using Four Wave Mixing in a Semiconductor Laser Amplifier," *Electron. Lett.,* **30**, 1938-1940 (1994).

10. K.L. Hall, and K.A. Rauschenbach, "100-Gbit/s Bitwise Logic," *Opt. Lett.,* **23**, 1271-1273 (1998).

11. N.J. Doran, and D. Wood, "Nonlinear-Optical Loop Mirror," *Opt. Lett.,* **13**, 56-58 (1988).

12. G.P. Agrawal, *Nonlinear Fiber Optics*, Academic Press, San Diego, CA, 1989.

13. M. Eiselt, W. Pieper, and H.G. Weber, "SLALOM - Semiconductor-Laser Amplifier in a Loop Mirror," *J. Lightwave Technol.*, **13**, 2099-2112 (1995).

14. J.P. Sokoloff, P.R. Prucnal, I. Glesk, and M. Kane, "A Terahertz Optical Asymmetric Demultiplexer (TOAD)," *IEEE Photon. Tech. Lett.*, **5**, 787-790 (1993).

15. J. Mark, and J. Mork, "Subpicosecond Gain Dynamics in InGaAsP Optical Amplifiers - Experiment and Theory," *Appl. Phys. Lett.*, **61**, 2281-2283 (1992).

16. J.P Sokoloff, I. Glesk, P.R. Prucnal, and R.K. Boncek, "Performance of a 50 Gbit/s Optical-Time Domain Multiplexed System Using a Terahertz Optical Asymmetric Demultiplexer," *IEEE Photon. Tech. Lett.*, **6**, 98-100 (1994).

17. I. Glesk, J.P. Sokoloff, and P.R. Prucnal, "Demonstration of All-Optical Demultiplexing of TDM Data at 250 Gbit/s," *Electron. Lett.*, **30**, 339-341 (1994).

18. D.D. Marcenac, A.E. Kelly, D. Nesset, and D.A.O. Davies, "Bandwidth Enhancement of Wavelength Conversion by Semiconductor Optical Amplifier Cascade," *Electron. Lett.*, **31**, 1442-1443 (1995).

19. D.A.O. Davies, "Small-Signal Analysis of Wavelength Conversion in Semiconductor-Laser Amplifiers via Gain Saturation," *IEEE Photon. Tech. Lett.*, **7**, 617-619 (1995).

20. J. Leuthold, C.H. Joyner, B. Mikkelsen, G. Raybon, J.L. Pleumeekers, B.I. Miller, K. Dreyer, and C.A. Burrus, "100 Gbit/s All-Optical Wavelength Conversion with Integrated SOA Delayed-Interference Configuration," *Electron. Lett.*, **36**, 1129-1130 (2000).

21. K.L. Hall, and K.A. Rauschenbach, "All-Optical Bit Pattern Generation and Matching," *Electron. Lett.*, **32**, 1214-1215 (1996).

22. M. Jinno, and T. Matsumoto, "Ultrafast All-Optical Logic Operations in a Nonlinear Sagnac Interferometer with 2 Control Beams," *Opt. Lett.*, **16**, 220-222 (1991).

23. A.J. Poustie, K.J. Blow, A.E. Kelly, and R.J. Manning, "All-Optical Binary Half-Adder," *Opt. Commun.*, **156**, 22-26 (1998).

24. A.J. Poustie, K.J. Blow, A.E. Kelly, and R.J. Manning, "All-Optical Full-Adder with Bit Differential Delay," *Opt. Commun.*, **168**, 89-93 (1999).

25. A.J. Poustie, K.J. Blow, A.E. Kelly, and R.J. Manning, "All-Optical Parity Checker with Bit-Differential Delay," *Opt. Commun.*, **162**, 37-43 (1999).

26. G. Theophilopoulos, K. Yiannopoulos, M. Kalyvas, C. Bintjas, G. Kalogerakis, H. Avramopoulos, L. Occhi, L. Schares, G. Guekos, S. Hansmann, and R. Dall' Ara, "40

GHz All-Optical XOR with UNI Gate," Paper MB2, *OFC '2001*, Anaheim, CA, March 17-22 (2001).

27. C. Bintjas, M. Kalyvas, G. Theophilopoulos, T. Stathopoulos, H. Avramopoulos, L. Occhi, L. Schares, G. Guekos, S. Hansmann, and R. Dall' Ara, "20 Gb/s All-Optical XOR with UNI gate," *IEEE Photonic. Techol. Lett.*, **12**, 834-836 (2000).

28. K.L. Hall, J.P. Donnelly, S.H. Groves, C.I. Fennelly, R.A. Bailey, and A. Napoleone, "40 Gbit/s All-Optical Circulating Shift Register with an Inverter," *Opt. Lett.*, **22**, 1479-1481 (1997).

29. A.E. Kelly, I.D. Phillips, R.J. Manning, A.D. Ellis, D. Nesset, D.G. Moodie, and R. Kashyap, "80 Gbit/s All-Optical Regenerative Wavelength Conversion Using Semiconductor Optical Amplifier based Interferometer," *Electron. Lett.*, **35**, 1477-1478 (1999).

30. K.E. Stubkjaer, "Semiconductor Optical Amplifier-Based All-Optical Gates for High-Speed Optical Processing," *IEEE J. Sel. Top. Quant. Electron.*, **6**, 1428-1435 (2000).

31. A.D. Ellis, A.E. Kelly, D. Nesset, D. Pitcher, D.G. Moodie, and R. Kashyap, "Error Free 100 Gb/s Wavelength Conversion Using Grating Assisted Cross Gain Modulation in a 2 mm Long Semiconductor Optical Amplifier," *Electron. Lett.*, **34**, 1958-1959 (1998).

32. D. Norte, and A.E. Willner, "Multistage All-Optical WDM-to-TDM-to-WDM and TDM-to-WDM-to-TDM Data-Format Conversion and Reconversion Through 80 km of Fiber and Three EDFAs," *IEEE Photon. Technol. Lett.*, **7**, 1354-1356 (1995).

33. J. Zhou, N. Park, J.W. Dawson, K.J. Vahala, M.A. Newkirk, and B.I. Miller, "Terahertz Four-Wave Mixing Spectroscopy for Study of Ultrafast Dynamics in a Semiconductor Optical Amplifier," *Appl. Phys. Lett.*, **63**, 1179-1181 (1993).

34. K. Uchiyama, S. Kawanishi, and M. Saruwatari, "100-Gb/s Multiple-Channel Output All-Optical OTDM Demultiplexing Using Multichannel Four-Wave Mixing in a Semiconductor Optical Amplifier," *IEEE Photonic. Technol. Lett.*, **10**, 890-892 (1998).

35. D.F. Geraghty, R.B. Lee, M. Verdiell, M. Ziari, A. Mathur, and K.J. Vahala, "Wavelength Conversion for WDM Communication Systems Using Four-Wave Mixing in Semiconductor Optical Amplifiers," *IEEE J. Sel. Top. Quant. Electron.*, **3**, 1146-1155 (1997).

36. D.D. Marcenac, D. Nesset, A.E. Kelly, M. Brierley, A.D. Ellis, D.G. Moodie, and C.W. Ford, "40 Gbit/s Transmission over 406 km of NDSF Using Mid-Span Spectral Inversion by Four-Wave Mixing in a 2 mm Long Semiconductor Optical Amplifier," *Electron. Lett.*, **33**, 879-880 (1997).

37. D. Cotter, J.K. Lucek, M. Shabeer, K. Smith, D.C. Rogers, D. Nesset, and P. Gunning, "Self-Routing of 100 Gbit/s Packets Using 6 Bit Keyword Address Recognition," *Electron. Lett.*, **31**, 1475-1476 (1995).

38. O. Kamatani, and S. Kawanishi, "Ultrahigh-speed Clock Recovery with Phase Lock Loop Based on Four-Wave Mixing in a Traveling-Wave Laser Diode Amplifier," *J. Lightwave Technol.*, **14**, 1757-1767 (1996).

Chapter 3

Four-Wave Mixing in Semiconductor Optical Amplifiers

3.1 Introduction

Four-Wave Mixing (FWM) is a third-order nonlinear process in which a polarization is created in a medium that depends on the product of three electric fields. The induced polarization leads to the creation of new frequency components of the electric field. In a semiconductor, the nonlinear polarization can be mediated by resonant interactions of the electric fields with the carriers in the medium [1]. Since resonant interactions lead to attenuation of light, the nonlinear products that are created have low intensities. One way to circumvent this problem is to use population inversion to create a gain in the medium [2]. A Semiconductor Optical Amplifier (SOA) can provide high gain (typically ~ 30 dB) which then amplifies the nonlinear mixing products that are created. FWM in SOAs has been studied extensively for wavelength conversion [3-6] and it has the advantage of being transparent to bit format. Furthermore, FWM in SOAs is an ultrafast nonlinear process with bandwidths that are well over a terahertz, since the contributions to the

nonlinear susceptibility include intraband carrier dynamics that are limited by the carrier-phonon and carrier-carrier scattering lifetimes which occur in the sub-picosecond regime.

In a typical FWM experiment, a strong pump wave at frequency ω_p and a probe wave at ω_q are combined and coupled to the waveguide modes of the SOA, which is a travelling wave amplifier. Dynamic gain and index gratings are formed due to the beating of the pump and probe waves, at a detuning frequency given by $\Omega = \omega_q - \omega_p$. The pump and the probe waves are subsequently scattered by these gratings which give rise to the FWM sidebands, as shown in Figure 3.1.

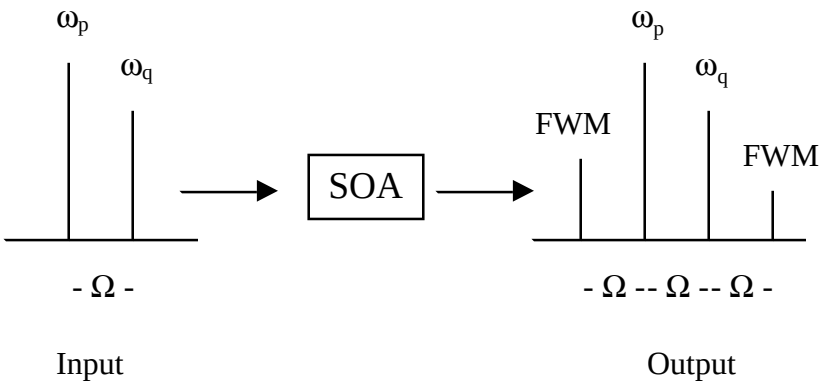

Figure 3.1: Generation of the FWM sidebands in a SOA

Consider the scattering process in which the pump and probe form a grating, which scatters the pump and gives rise to one of the FWM sideband as shown in Figure 3.1. The frequency of this component is $\omega_{FWM} = \omega_p - \Omega$ or $\omega_{FWM} = \omega_p + \Omega$. When

$\omega_p > \omega_q$, the FWM signal has a higher frequency than the probe (or is wavelength downshifted) and when $\omega_p < \omega_q$, the FWM signal has a lower frequency than the probe (or is wavelength upshifted). In the copropagation FWM geometry, guided waves in the SOA are given by $E_j(z)\exp\left[i\left(k_j z - \omega_j t\right)\right]$, where $j = p,q,c$ indicate the pump, probe and converted signal respectively; $\{E_j(z)\}$ are the field amplitudes and z is the longitudinal coordinate along the propagation axis of the SOA. Then electric field of the FWM component generated can be written as

$$E_c(z) = \chi^{(3)}(\Omega)E_p^2(z)E_q^*(z)e^{i\Delta kz}, \tag{3-1}$$

where $\chi^{(3)}(\Omega)$ is the third-order nonlinear susceptibility which depends on the detuning frequency, Ω, between the pump and the probe; and $\Delta k = 2k_p - k_q - k_c$ is the wave-vector phase mismatch between the pump, probe, and the converted signal. In a SOA, the free-space wave-vectors are replaced with the propagation vectors of the waveguide modes for the pump, probe, and the converted signal.

3.2 Contributions to the FWM Susceptibility

For detuning frequencies less than a few gigahertz, the largest contribution to the FWM susceptibility is due to carrier density modulation (CDM) which arises from the beating of the pump and probe waves. The intensity beating due to the pump and the probe lead

to a pulsation of the population inversion in the medium. This pulsation of the total carriers leads to a gain modulation as seen by the traveling waves, which gives rise to the FWM sidebands. Due to the slow recovery of the carrier density, determined by the carrier lifetime, τ_s, which is on the order of several hundred picoseconds, the efficiency of FWM mediated by CDM drops off for frequency detunings much larger than 10 GHz.

At large detuning frequencies, the gain and index gratings are formed by intraband processes, such as carrier heating (CH) and Spectral Hole Burning (SHB) [7, 8]. Instead of a pulsation of the total carriers in the conduction and valence bands of the semiconductor, the occupation probabilities of the individual transition levels are modulated to form the gain and index gratings that give rise to the FWM sidebands. The pulsation of the occupation probabilities create distortions in the equilibrium Fermi distribution functions of the carriers, which relax back to their equilibrium state through different scattering processes, such as CH and SHB. SHB arises from carrier-carrier scattering which tend to restore a quasi-equilibrium Fermi distribution function. Typically, carriers scatter each other at a time scale, τ_{SHB}, which is of the order of 50-100 femtoseconds. The quasi-equilibrium Fermi distribution function is characterized by a temperature which is different from the lattice temperature. The relaxation to the lattice temperature is through the emission of optical phonons with a time constant due to carrier-phonon scattering lifetime, τ_{CH}, which is of the order of 0.5-1 picoseconds. Thus the relaxation of the carriers can be explained as a three step process: (1) the carriers first scatter with each other to create a quasi-equilibrium Fermi distribution which has a temperature T_x that is different from the lattice temperature (SHB), (2) the temperature of

the carriers then relaxes to the lattice temperature through carrier-phonon scattering (CH) and (3) the carriers then recombine through stimulated recombination.

The total FWM susceptibility due to these contributions can be derived by solving the density matrix equations for the occupation probabilities and the polarization of the levels that are resonant with the electric fields launched into the SOA, and in the presence of the relaxation processes mentioned above. A rigorous derivation of the FWM susceptibility is presented by Uskov *et al.* [8] that can be given by the expression

$$\chi^{(3)}(\Omega) = \left[\frac{A_{CDM} e^{i\phi_{CDM}}}{(1 - i\Omega\tau_s)} + \frac{A_{CH} e^{i\phi_{CH}}}{(1 - i\Omega\tau_{CH})(1 - i\Omega\tau_{SHB})} + \frac{A_{SHB} e^{i\phi_{SHB}}}{(1 - i\Omega\tau_{SHB})} \right], \tag{3-2}$$

where A_{CDM}, A_{CH} and A_{SHB} are constants that determine the strength of the scattering process leading to the nonlinearity, and ϕ_{CDM}, ϕ_{CH} and ϕ_{SHB} are the phase factors due to the scattering processes. The frequency dependence of $\chi^{(3)}(\Omega)$ was first measured by Zhou *et al.* [9]. The observed difference in the conversion efficiencies for positive and negative detuning frequencies of the pump and the probe was attributed to the interference between the terms arising from different scattering mechanisms. A typical FWM response for wavelength downshift measured in a 1.5 mm long bulk SOA is shown in Figure 3.2.

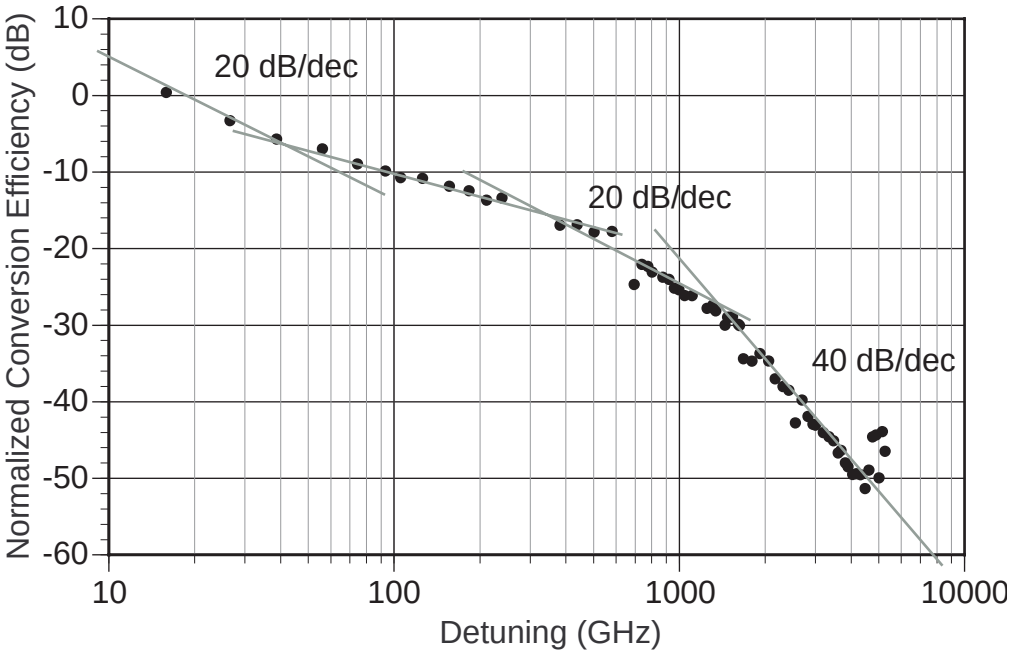

Figure 3.2: Conversion efficiency of the FWM signal measured for wavelength downshift in a 1.5 mm bulk SOA

3.3 Conversion Efficiency of FWM in a SOA

The FWM conversion efficiency is defined as the ratio of the intensity of the FWM signal at the output of the SOA to the intensity of the probe wave that is launched into the SOA. The total conversion efficiency at the output of the SOA can be derived by using a lumped model as proposed by Zhou *et al.* [10] and solving the coupled propagation equations for each frequency component of the travelling waves that can be written as

$$\frac{dE_{p,q}(z)}{dz} = \frac{1}{2}\left[\frac{g_0}{\left(1+\frac{P(z)}{P_{sat}}\right)}(1-i\alpha)-\alpha_l\right]E_{p,q}(z) \tag{3-3a}$$

$$\frac{dE_c(z)}{dz} = \frac{1}{2}\left[\frac{g_0}{\left(1+\frac{P(z)}{P_{sat}}\right)}(1-i\alpha)-\alpha_l\right]E_c(z)-\kappa(z)E_p^2(z)E_q^*(z)e^{i\Delta kz} \tag{3-3b}$$

$$P(z) = \left|E_p(z)\right|^2 + \left|E_q(z)\right|^2 + \left|E_c(z)\right|^2, \tag{3-3c}$$

where $\kappa(z)$ is the FWM coupling constant, g_0 is the unsaturated gain coefficient, P(z) is the total optical power at position *z* along the propagation axis of the waveguide, P_{sat} is the saturation power of the SOA, α is the linewidth enhancement factor [11] and α_l is the nonsaturable internal loss per unit length of the waveguide. Zhou *et al.* showed that $\kappa(z)$ could be written as

$$\kappa(z) = \frac{1}{2}\frac{g_0}{\left(1+\frac{P(z)}{P_{sat}}\right)}\sum_{m=1}^{3}\frac{1-i\alpha_m}{1-i\Omega\tau_m}\cdot\frac{1}{P_m}, \tag{3-4}$$

where m=1, 2, 3 denote CDM, CH and SHB. $\{\tau_m\}$ and $\{P_m\}$ are the lifetimes and saturation powers associated with these mechanisms and $\{\alpha_m\}$ are the ratios between the real and imaginary parts of the refractive index change induced by these mechanisms. Solving the coupled equations under moderate saturation, the expression for the

conversion efficiency, η, with phase-matching conditions satisfied at the output of the SOA was derived as

$$\eta(\Omega) = 10\log_{10}\frac{P_c(L)}{P_q(0)} = 3G + 2I_p + 20\log_{10}\left|\sum_{m=1}^{3} c_m \cdot \frac{1}{1 - i\Omega\tau_m}\right|, \tag{3-5}$$

where L is the length of the SOA, I_p is the input pump power in dBm, G is the saturated gain of the SOA in dB and is given by

$$G = \exp\left[\int_0^L \left(\frac{g_0}{\left(1 + \frac{P(z)}{P_{sat}}\right)} - \alpha_l\right) dz\right] \tag{3-6a}$$

$$G(dB) = 4.34\int_0^L \left[\frac{g_0}{\left(1 + \frac{P(z)}{P_{sat}}\right)} - \alpha_l\right] dz, \tag{3-6b}$$

The importance of the length of the SOA in determining the conversion efficiency of the FWM signal was investigated by Mecozzi *et al.* [5, 12]. Under the assumption of perfect phase-matching, an analytical expression for the conversion efficiency was derived and they showed that for frequencies exceeding 10 GHz, i.e., $\Omega\tau_s >> 1$, the conversion efficiency can be written in the form

$$\eta(\Omega) = \frac{\left|E_c(L)\right|^2}{\left|E_q(0)\right|^2} = \left[\frac{P_p(0)}{P(0)}\right]\frac{\left|R(\Omega)\right|^2}{(1+\varepsilon P_{sat})}\left(\ln\frac{G_0}{G}\right)^2 G, \tag{3-7}$$

where L is the length of the SOA, $G_0 = G_0(L)$ is the unsaturated gain (or small signal gain) of the SOA while G is the saturated gain of the SOA given by Eqn. (3-6a), ε is the gain compression coefficient and R(Ω) is the frequency response function of the FWM process due to the different scattering processes. Since the small signal gain, G_0 neglects saturation effects, it is expressed as

$$G_0 = \exp\left[\int_0^L (g_0 - \alpha_l)dz\right] = \exp\left[(g_0 - \alpha_l)L\right], \tag{3-8}$$

The conversion efficiency strongly depends on the length of the device through saturation of the SOA. The saturated gain G can be expressed in the same form as Eqn. (3-8) with an effective length L_{eff} over which transparency (no gain or loss seen by the travelling waves) is achieved, i.e.,

$$G = \exp\left[\int_0^{L_{eff}} (g_0 - \alpha_l)dz\right] = \exp\left[(g_0 - \alpha_l)L_{eff}\right], \tag{3-9}$$

With these expressions, keeping all other parameters constant, the dependence of the conversion efficiency versus the length of the SOA is of the form,

$$\eta(L) \propto \left(g_0 - \alpha_l\right)^2 \left(L - L_{eff}\right)^2 \tag{3-10a}$$

$$\eta(dB) = C + 10\log_{10}(L - L_{eff})^2, \tag{3-10b}$$

where C is a constant. High conversion efficiencies can thus be obtained by using longer SOAs that operate in the gain saturation regime. L_{eff} can be made smaller by strongly amplifying the input waves before coupling them into the SOA waveguide. Thus the SOA operates in transparency over most of the propagation length. Using longer SOAs provides longer interaction length over which FWM can occur leading to higher conversion efficiencies. At low detuning frequencies, the nonlinearities can be high from the large conversion efficiencies, gain and longer interaction lengths. Figure 3.3 shows many cascaded FWM processes that occur in a 1.5 mm SOA when two waves P1 and P2 are launched with a detuning of ~ 0.15 nm (or close to 18 GHz).

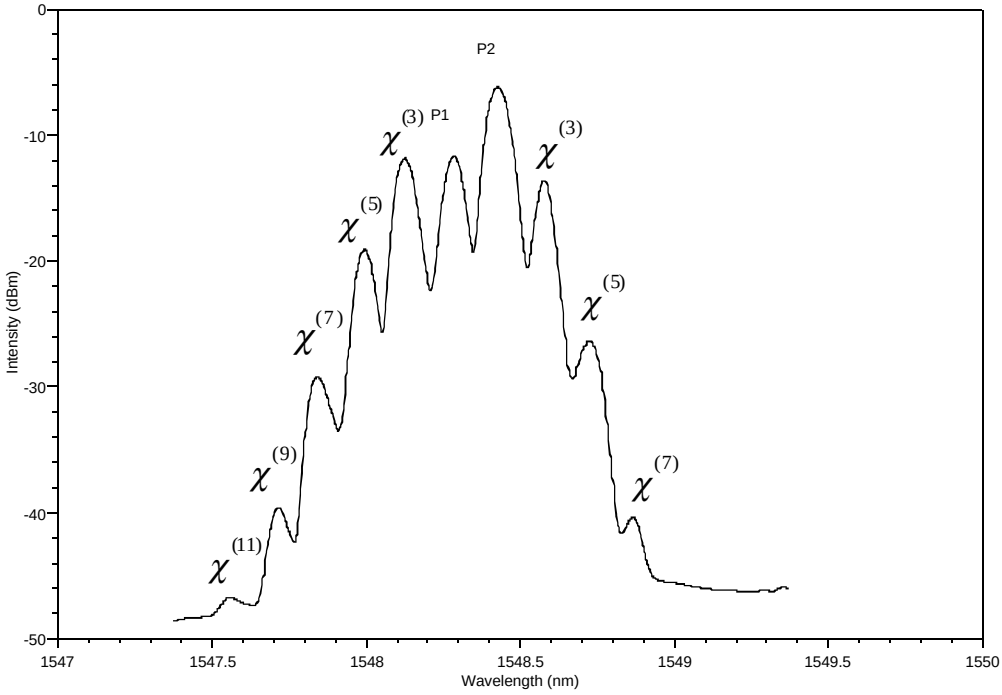

Figure 3.3: Many cascaded FWM processes can occur due to high nonlinearity in a SOA when two waves P1 and P2 are launched

The above expressions are valid when phase matching between the wave-vectors of the different frequencies is satisfied ($\Delta k = 0$). For broadband wavelength conversion (detunings in the terahertz regime), phase matching is not necessarily satisfied and has to be included in the expressions derived above. The expression for the conversion efficiency is modified to

$$\eta(L) \propto (g_0 - \alpha_l)^2 (L - L_{eff})^2 \left[\frac{Sin^2\left(\frac{\Delta kL}{2}\right)}{\left(\frac{\Delta kL}{2}\right)^2} \right], \qquad (3\text{-}11)$$

where $\Delta k = 2k_p - k_q - k_c$, and is a function of the detuning frequency, Ω. The effect of phase matching on the conversion efficiency was measured for a 2.2 mm and a 4 mm long SOA and is shown in Figure 3.4.

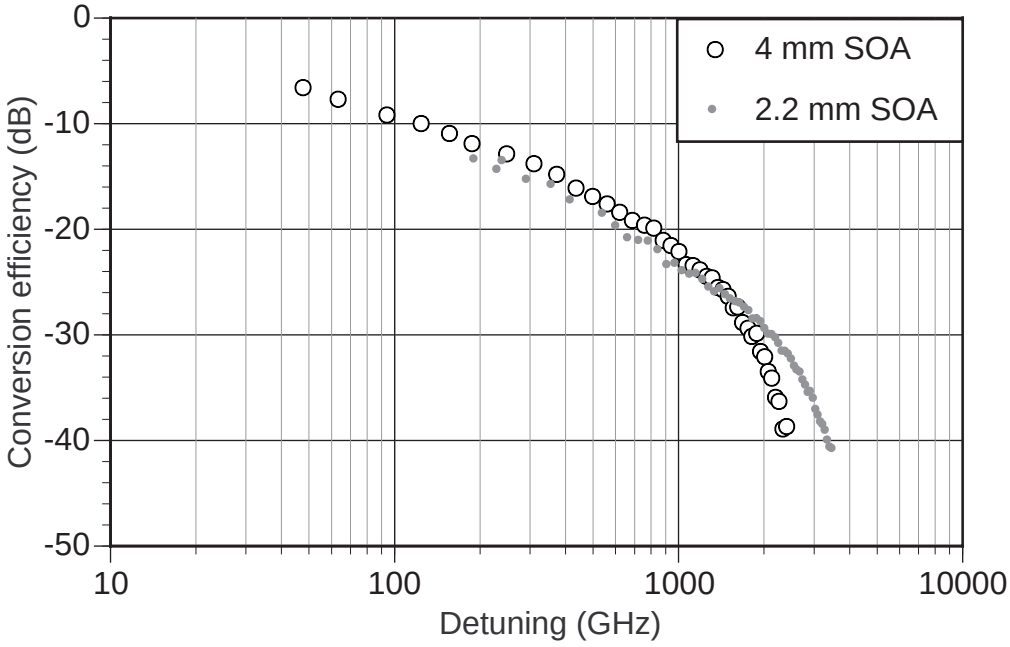

Figure 3.4: Conversion efficiency versus detuning for a 2.2 mm and 4 mm long SOA. The SOAs are biased at 1 A

3.4 Optical-Signal-to-Noise-Ratio of the FWM Signal

Due to the high FWM conversion efficiencies possible by strongly saturating the SOA, FWM is an ideal candidate for wavelength conversion since it has the advantage of being transparent to bit-format. Another important requirement for implementation of SOAs in

real systems is the Optical-Signal-to-Noise-Ratios (OSNR) on the converted signals. Since the SOA is composed of a gain medium, Amplified Spontaneous Emission (ASE) can severely degrade the OSNR of the converted signal. OSNR can be increased by strongly saturating the SOA [13]; thereby the ASE is generated over a very small length of the device while the mixing occurs in the transparency region. The ASE in a bandwidth $\Delta\nu$ is given by the expression

$$\text{ASE} = (G-1)\, h\nu\, \Delta\nu, \tag{3-12}$$

where h is the Planck's constant, ν is the frequency, and G is the saturated gain of the SOA. From Equations (3-7), (3-10a) and (3-12) the expression for the OSNR can also be written as

$$OSNR(L) \propto (g_0 - \alpha_l)^2 (L - L_{eff})^2 \left[\frac{Sin^2\left(\frac{\Delta kL}{2}\right)}{\left(\frac{\Delta kL}{2}\right)^2} \right]. \tag{3-13}$$

Thus longer devices operating under saturation are key to successful systems applications. The small-signal gain coefficient can be written as $g_0 = a_0(n - n_0)$, where n is the injection carrier density and n_0 is the carrier density needed to offset the intrinsic losses of the SOA waveguide. Higher conversion efficiency and OSNR can be obtained by increasing the carrier density in the active region of the SOA.

3.5 Broad-band Wavelength Conversion Using Long SOAs

Long SOAs were fabricated to study conversion efficiencies at large detunings and obtain high OSNR for broad-band wavelength conversion. A 2.2. mm long compressively strained quantum well SOA was tested under high injection current (1 Amp). Figure 3.5 shows a 40 nm wavelength downshift with a 23.2 dB OSNR in a 0.1 nm Resolution Bandwidth, which is sufficient for error free detection (Bit Error Rate < 10^{-9}) on the converted signal [14].

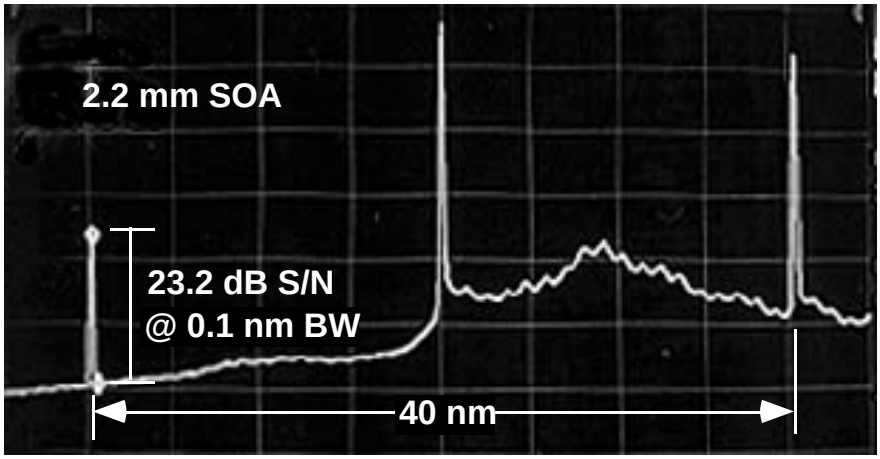

Figure 3.5: 40 nm downshift in a 2.2 mm long SOA with 23.12 dB OSNR for low error-rate detection at 10 Gb/s (from Ref. [14])

3.6 Polarization Dependence of FWM

FWM is sensitive to the states of polarization (SOP) of the electric fields of the pump and the probe. The FWM susceptibility is a tensor of rank four and the FWM process can be written as

$$E_i^{(c)} = \chi_{ijkl}^{(3)}(\Omega) E_j^{(p)} E_k^{(p)} E_l^{(q)*}. \tag{3-14}$$

The susceptibility tensor in a semiconductor can be derived from the matrix elements of the dipole transitions between the valence and conduction bands. A detailed calculation by Paiella *et al.* [15, 16] shows that the FWM susceptibility can be written as

$$\chi_{ijkl} = \left(\sum_{c,v} \mu_i^{vc} \mu_j^{cv} \right) \left(\sum_{c',v'} \mu_k^{c'v'} \mu_l^{v'c'} \right) (\chi_{CDM} + \chi_{CH}) + \left(\sum_{c,v,c',v'} \mu_i^{vc} (\mu_j^{cv'} \mu_k^{c'v} + \mu_j^{c'v} \mu_k^{cv'}) \mu_l^{v'c'} \right) \frac{\chi_{SHB}}{2} \tag{3-15}$$

The Bloch states of the heavy and light hole valence bands in III-V semiconductors can be written in terms of the total angular momentum eigenstates $\left|\frac{3}{2}, \pm\frac{3}{2}\right\rangle$ and $\left|\frac{3}{2}, \pm\frac{1}{2}\right\rangle$. Based on these eigenstates the general solution of the coupled mode equations of FWM can be written in the form [16]

$$E_i^{(s)}(L) = \left(E^{(p)}(0)\right)^2 \left(E^{(q)}(0)\right)^* \left[\sum_{k=1}^{2} \left(p_i M_{iikk} p_k q_k^* \right) + M_{ilil}\big|_{l \neq i} p_l p_i q_l^* + M_{illi}\big|_{l \neq i} p_l^2 q_i^* \right], \tag{3-16}$$

where p_i (q_i) are the *i*-th component of the polarization vector of the pump (probe) waves, $M_{ijkl} = \chi_{ijkl} R_{ijkl}$, where R_{ijkl} is a propagation factor that accounts for the birefringence, gain anisotropy and wavelength dependence on the gain coefficient and refractive index of the SOA. The first term arises from the beating of the same components of the pump and the probe, i.e., the TE (TM) component of the pump can form a grating only the TE (TM) of the probe. The TE (TM) component of the pump can then be scattered by these gratings into a FWM signal into the TE (TM) direction. This is true for CDM and CH processes which are predominant in the sub-terahertz detuning range, and the ordinary SHB process, which involves the modulation of the occupation probabilities of the electronic states. For CDM and CH, the formation of the gratings and the subsequent scattering of the pump into the FWM sideband are two distinct processes which can involve different transition levels as indicated by the first term in Equation (3-15). In the terahertz detuning range, where SHB is the dominant mechanism, gratings can also be formed between the orthogonal TE and TM modes of the pump and the probe through the modulation of relative coherence between the initial state and the second intermediate state with opposite spin. These gratings then scatter the pump into FWM sidebands with orthogonal polarization (given by the other terms in Equation (3-16)). However, in the sub-terahertz regime, the contribution from the first term in Equation (3-16) dominates and the other terms can be neglected. In general, the contribution from the last two terms in Equation (3-16) can be much smaller than the first one due to birefringence in the waveguide structure.

Bibliography

1. R.W. Boyd, *Nonlinear Optics*, Academic Press, London, UK, 1992.

2. J. Reintjes, and L.J. Palumbo, "Phase Conjugation in Saturable Amplifiers by Degenerate Frequency Mixing," *IEEE J. Quantum Electron.*, **QE-18**, 1934-1940 (1982).

3. D. Campi, and C. Corriaso, "Wavelength Conversion Technologies," *Photonic. Netw. Commun.*, **2**, 85-95 (2000).

4. D.F. Geraghty, R.B. Lee, M. Verdiell, M. Ziari, A. Mathur, and K.J. Vahala, "Wavelength Conversion for WDM Communication Systems using Four-Wave Mixing in Semiconductor Optical Amplifiers," *IEEE J. Sel. Top. Quant. Electron.*, **3**, 1146-1155 (1997).

5. A. D'Ottavi, F. Girardin, L. Graziani, F. Martelli, P. Spano, A. Mecozzi, S. Scotti, R. Dall 'Ara, J. Eckner, and G. Guekos, "Four-Wave Mixing in Semiconductor Optical Amplifiers: A Practical Tool for Wavelength Conversion," *IEEE J. Sel. Top. Quant. Electron.*, **3**, 522-528 (1997).

6. S.J.B. Yoo, "Wavelength Conversion Technologies for WDM Network Applications," *J. Lightwave Technol.*, **14**, 955-966 (1996).

7. G.P. Agrawal, "Population Pulsation and Nondegenerate Four-Wave Mixing in Semiconductor Laser Amplifiers," *J. Opt. Soc. Am. B*, **5**, 147-159 (1988).

8. A. Uskov, J. Mork, and J. Mark, "Wave Mixing in Semiconductor Laser Amplifiers due to Carrier Heating and Spectral-Hole Burning," *IEEE J. Quantum Elect.*, **30**, 1769-1781 (1994).

9. J.H. Zhou, N. Park, J.W. Dawson, K.J. Vahala, M.A. Newkirk, and B.I. Miller, "Terahertz Four-Wave Mixing Spectroscopy for Study of Ultrafast Dynamics in a Semiconductor Optical Amplifier," *Appl. Phys. Lett.*, **63**, 1179-1181 (1993).

10. J.H. Zhou, N. Park, J.W. Dawson, K.J. Vahala, M.A. Newkirk, and B.I. Miller, "Efficiency of Broad-band Four-Wave Mixing Wavelength Conversion using Semiconductor Traveling-Wave Amplifiers," *IEEE Photonic. Tech. Lett.*, **6**, 50-52 (1994).

11. C.H. Henry, "Theory of the Linewidth of Semiconductor Lasers," *IEEE J. Quantum Electron.*, **QE-18**, 259-264 (1982).

12. A. Mecozzi, "Analytical Theory of Four-Wave Mixing in Semiconductor Amplifiers," *Opt. Lett.*, **19**, 892-894 (1994).

13. A. D'Ottavi, P. Spano, G. Hunziker, R. Paiella, R. Dall 'Ara, G. Guekos, and K.J. Vahala, "Wavelength Conversion at 10 Gb/s by Four-Wave Mixing over a 30-nm Interval," *IEEE Photon. Tech. Lett.*, **10**, 952-954 (1998).

14. K. Vahala, R. Paiella, G. Hunziker, A. Bhardwaj, D. Dougherty, and U. Koren, "Ultrafast Dynamics in Quantum Well Semiconductor Optical Amplifiers and Applications," Paper WB1, *Topical Meeting on Optical Amplifiers and their Applications*, Vail, Colorado, July 27-29, 1998.

15. R. Paiella, G. Hunziker, U. Koren, and K.J. Vahala, "Polarization-Dependent Optical Nonlinearities of Multiquantum-Well Laser Amplifiers Studied by Four-Wave Mixing," *IEEE J. Sel. Top. Quant.*, **3**, 529-540 (1997).

16. R. Paiella, G. Hunziker, J.H. Zhou, K.J. Vahala, U. Koren, and B.I. Miller, "Polarization Properties of Four-Wave Mixing in Strained Semiconductor Optical Amplifiers," *IEEE Photon. Tech. Lett.*, **8**, 773-775 (1996).

Chapter 4

Advanced All-Optical Logic on a Spectral Bus

4.1 The Spectral Data Bus

Data transfer within a computer or between computers and its peripherals is done using a parallel architecture, where byte-wide (or bit-parallel) transmission is used. A byte, which is composed of several bits, is transmitted in one time slot using a data bus. Typically the data-bus is made using a ribbon of electrical cables. Within a computer, the data-bus forms a computer back-plane, over which data is transferred between different processing units. The parallel architecture is also more suitable for the transfer of data between computers, since it eliminates the need for serializer/deserializer circuits which can be expensive as the processing speeds increase. Transfer of data between processors using efficient protocols using byte-wide transmission over shared computer back-planes is essential for Massively Parallel Processing (MPP) [1]. The throughput of future computer networks for ultra high-speed distributed computing over a cluster of supercomputers will be limited by the speed with which data can be transferred over the data bus. One way to increase the transfer rate is to simply replace the electrical wires in the data-bus with optical fibers to form a multifiber ribbon [2, 3]. However, multifiber ribbons are not

practical for long-distance links since they can be very expensive and it is difficult to correct for bit-skew that can arise between different fibers of the ribbon. One possible approach is to use serial transmission over the optical fiber instead of byte-wide transmission. This would require the need for serializer/deserializer circuits at the transmitting and receiving ends of the optical fiber to maintain the bit-parallel format at the processing ends. As processor speeds increase, such circuits can be very expensive. Furthermore, the speed at which these circuits operate determine the "electronic bottleneck", i.e., the ultimate speed over which the cluster can operate.

The Spectral Data Bus was proposed by Loeb *et al*. [4] to increase the throughput of high-speed links between computers using optical fibers while maintaining the bit-parallel format for data transfer. Unlike conventional WDM systems, where the data on different wavelength channels is uncorrelated, the spectral data bus assigns each bit of the byte to be transmitted on a separate wavelength channel, as shown in Figure 4.1. Thus in one time slot, the entire byte is transmitted in parallel over different WDM channels. This approach eliminates the need for expensive serializer/deserializer circuits and multifiber ribbons. The individual bits can be recovered using all-optical filters, which isolate single WDM channels. Recent advances in optical device technology enable the integration of WDM components such as multi-wavelength laser arrays [5-8], wavelength multiplexers/demultiplexers [9-11] and photodiode arrays [12-14] on a single chip. Thus the WDM bus replaces a serial link by trading the serializer/deserializer for wavelength multiplexers/demultiplexers and trading the high-speed circuits for low-speed multiple circuits in an array. The major limitation to the implementation of the spectral data bus is the bit-skew that arises from fiber group velocity dispersion between different

wavelengths. However, techniques to compensate for dispersion, such as using dispersion compensating fiber [15], chirped fiber gratings [16], or phase conjugation [17] have been developed. Consequently, there has been an increased interest in realizing the potential attributes of the spectral bus [1, 18-19].

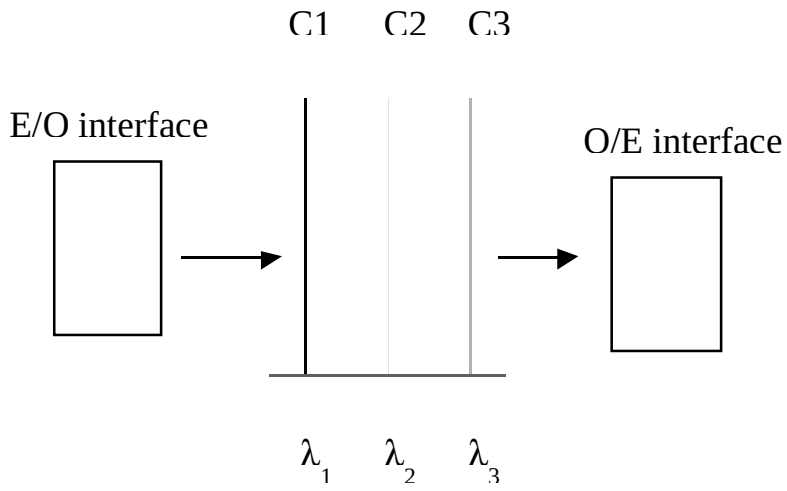

Figure 4.1: Schematic of the Spectral Data Bus for byte-wide transmission (C1, C2, C3 etc. are different WDM channels)

4.2 All-Optical Front-End Processing on the Spectral Bus

There are various front-end signal-processing possibilities associated with the spectral bus, including byte-wide error correction and detection. A front-end device is defined as one that is located between the bus and whatever the bus is linked to (presumably a

computer through an optoelectronic interface). The throughput of a computer network can be further increased by moving some of the front-end digital processing functions to the all-optical domain. Thus, all-optical front-end devices on both the transmitting and receiving ends of the spectral bus as shown in Figure 4.2 could be realized. One example of such devices could be to implement coding and decoding for error detection and correction [20] or encryption for improved security.

In this very limited context, a form of optical logic based on Four-Wave Mixing (FWM) designed to process data on-the-fly in the spectral form is proposed and studied. Since FWM involves a third-order nonlinearity, a Non-Degenerate Four-Wave Mixing (ND-FWM) process can involve a simultaneous interaction between three different frequencies of light. Thus, up to three bits can be multiplied on the spectral bus using ND-FWM. So, in principle, a three-bit Boolean operation is possible. ND-FWM on intensity modulated data offers a simple "AND" operation between three bits and cannot be easily generalized to implement other Boolean functions. However, if the information on each bit is encoded in the State of Polarization (SOP) of the electric field rather than the intensity of the WDM channel, the polarization-selection rules of the ND-FWM process can be exploited to incorporate more versatile Boolean functions, since the SOP of the FWM output is sensitive to the SOPs of all the fields involved in the mixing process.

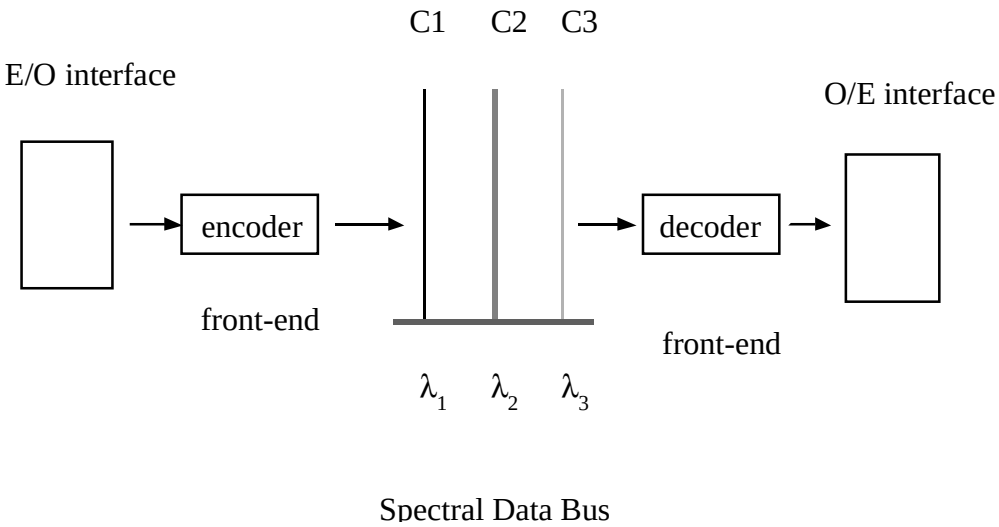

Figure 4.2: All-optical logic circuits can be designed for some form of limited on-the-fly front-end signal processing on a spectral bus (C1, C2, C3 etc. are different WDM channels)

4.3 Polarization Shift Keying (PolSK)

The idea of encoding binary information on the state of polarization of the electric field for transmission is not new. Polarization Shift Keying (PolSK) was proposed by Benedetto *et al*. [21] for data transmission in long-haul networks, where information is coded on a set of Stokes parameters that describe the electric field vector while the amplitude of the electric field is kept constant. In this case, the Stokes parameters would form a vector that would lie on a Poincaré sphere. In general, a mapping between m-ary (m logic states) coded information with a constellation of m points on the Poincaré sphere can be found [21]. It was further noted that when a polarized lightwave is sent through a

single-mode optical fiber, the SOPs of the electric fields are altered due to the presence of birefringence over the transmission path. However, the fiber birefringence only causes a rigid rotation of all the vectors on the Poincaré sphere and the spatial relationship between the different vectors is preserved. Thus the birefringence would only cause a uniform rotation of the entire constellation, assuming that polarization dependent gain or loss were absent in the system. As a result, the PolSK coded information remains uncorrupted and can be recovered with the design of suitable receivers that can recover the Stokes parameters and decode the coded information electronically from the Stokes parameters [22].

A simple example is binary PolSK (or 2-PolSK), where the "1" and "0" states are represented by orthogonal linear states of polarization of the electric field, as shown in Figure 4.3.

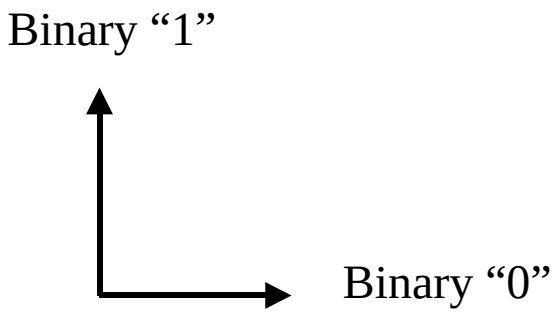

Figure 4.3: 2-PolSK coding using orthogonal linear states of polarization

System demonstrations of data transmission using 2-PolSK are predicted to have lower power penalties compared to data transmission using intensity modulation [21, 22]. Higher extinction ratios and signal to noise ratios using 2-PolSK over intensity modulation were experimentally demonstrated using a differential heterodyne detection scheme [23, 24]. It was also shown that PolSK modulation is less sensitive to phase noise of the transmitting lasers in comparison with other coherent transmission schemes [25]. Furthermore, since PolSK modulated electric fields have a constant amplitude, the effects of Self-Phase Modulation (SPM) are absent in comparison to intensity modulation (IM-DD systems) where SPM leads to pulse broadening which limits the bit rate over which information can be transmitted.

The polarization states of the PolSK coded electric field is naturally scrambled in comparison with IM-DD systems in which system performance can be degraded due to polarization-hole-burning in EDFAs [26], where the signal experiences a lower gain than the ASE noise copropagating in the orthogonal direction. PolSK modulation is immune to polarization-hole-burning effects. Though 2-PolSK would be affected by Polarization Mode Dispersion (PMD), it has been argued that for ultra long-haul transmission systems, the pulse broadening due to SPM in IM-DD systems is larger than the broadening of PolSK coded pulse due to Polarization Mode Dispersion (PMD). Thus, long-haul data transmission using PolSK modulation has many advantages to be of practical interest.

Though 2-PolSK transmission over single-mode optical fiber requires special receivers to recover the Stokes parameters, direct detection can be employed with the use of Polarization Maintaining (PM) fiber. A PM fiber uses an asymmetric core, which

breaks the degeneracy between its orthogonal modes thereby reducing the coupling of power between the modes. Thus, if the orthogonal linear states of polarization representing the binary "1" and "0" are aligned along the fast and slow axes (or principal axes) of the PM fiber, mode coupling between the orthogonal modes is minimized in the presence of birefringence. The SOPs of the "1" and "0" states would remain strictly aligned along the principal axes of the PM fiber over the entire transmission length. In this case, direct detection can be employed by simply inserting a polarizer correctly aligned to the fast (or slow) axis of the PM fiber before the photodetector.

Though the installation of PM fiber for long-haul transmission (especially trans-oceanic transmission) seems unlikely in the very near future due to the high costs involved, PM fiber offers a solution to circumvent PMD effects that occur in a single mode fiber. The advantages of using 2-PolSK modulation using PM fibers could also be realized for the different WDM channels of a spectral data bus.

4.4 All-Optical Processing on PolSK Coded Spectral Data

2-PolSK coding over a spectral bus using PM fiber is particularly attractive for implementing limited front-end all-optical processing based on the polarization selection rules of FWM for shared computer back-plane applications where the optical power in each WDM channel is sufficiently high. One possible application is the design of all-optical coding and decoding circuits for error detection and correction. As a simple example, a circuit that performs error detection and correction on a (3,1) Hamming Code

is designed to illustrate the potential offered by the proposed scheme. It is shown that the PolSK coding and byte-wide format can be maintained using this scheme, which makes it possible to generalize the scheme to enable more sophisticated Boolean operations involving higher-level Hamming Codes.

4.5 Coding and Decoding Using the (3,1) Hamming Code

The (3,1) Hamming Code is the simplest of a class of linear Forward Error-Correcting Codes (FECs) as proposed by R.W. Hamming [27], which allow for single error-correction. FECs are based on adding redundancy to the information being transferred. This can then be used to correct for errors that can occur from the corruption of data while transmitting over a noisy channel. For serial transmission, the added redundancy comes with a cost of reduced channel speed while for a parallel architecture involving byte-wide transmission, the channel speed can be maintained by increasing the word length and adding more channels (more wavelength channels in case of the spectral bus).

The (3,1) Hamming Code allows for single error correction at a time by transmitting each data bit with two check-bits with the same value. Thus the 3-bit word is transmitted as a vector [0,0,0] or [1,1,1]. Single error correction is possible if the Hamming distance (defined as the number of bits that differ between two legitimate code words) is greater than or equal to 3 ($2m+1$ with $m=1$ for one error). Furthermore, the probability of two errors occurring simultaneously in the 3-bit word is far less than the probability of one error occurring in the 3-bit word. For example, consider the case when

the transmitted word is [1,1,1] and the data-bit is corrupted over the channel so that the received word is [0,1,1]. It is still possible to extract the information that was transmitted (i.e., the 3-bit word was a [1,1,1]) by taking a "majority poll" of the bits in the 3-bit word. The truth table for the (3,1) Hamming code is given in Table 4.1, where C1, C2, and C3 denote the channels that carry the data and check-bits, and EC denotes the error corrected output. The (3,1) Hamming Code can also be interpreted as a projection of the $2^3 = 8$ possible 3-bit words on the two originally transmitted 3-bit words [0,0,0] or [1,1,1] which can be visualized using the cube shown next to the table in Figure 4.4. Thus a single error creates a new word which lies on the edge of the cube containing the original code word. Thus the Hamming distance from the correct code word is one, while its Hamming distance from the incorrect code word is two.

C1	C2	C3	EC
1	1	1	1
0	0	0	0
1	1	0	1
1	0	1	1
0	1	1	1
0	0	1	0
0	1	0	0
1	0	0	0

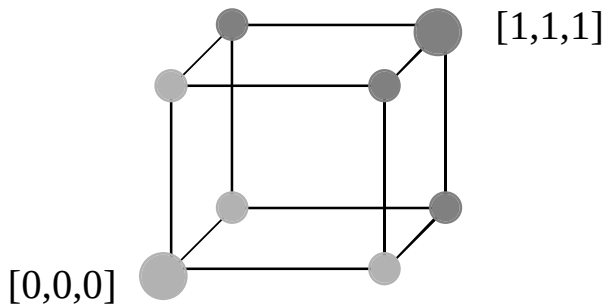

Figure 4.4: Truth table and pictorial representation of the (3,1) Hamming Code

The Boolean function for this truth table can be written as in Equation (4-1),

$$EC = (C1 \cap C2) \cup (C2 \cap C3) \cup (C1 \cap C3) \tag{4-1}$$

where "$\cap$" denotes the Boolean "AND" function and "$\cup$" denotes the Boolean "OR" function. An implementation of the Boolean function in terms of the standard 2-input "AND" and "OR" gates is shown in Figure 4.5.

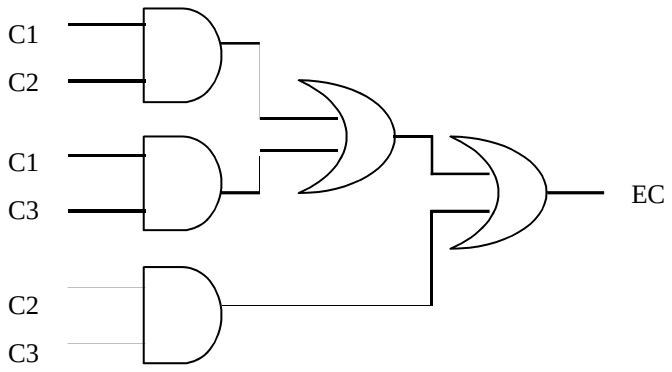

Figure 4.5: Implementation of the Boolean function for the (3,1) Hamming Code using 2-input "AND" and "OR" gates

We now proceed to design an error-correcting circuit for the (3,1) Hamming Code just described, based on the polarization properties of ND-FWM.

4.6 Polarization Properties of ND-FWM Between 2-PolSK Coded WDM Channels

Assuming that the 3-bit word is PolSK coded in a byte-wide format, the front-end decoder circuit can receive a combination of 2^3=8 possible inputs, as shown in the table in Figure 4.4, and should produce a unique output for each case. The polarization selection rules of the ND-FWM process between three different wavelength channels that carry 2-PolSK coded information can be used to implement the Boolean function for error correction. If the bits are placed on spectral channels C1, C2 and C3 the ND-FWM process creates an error-corrected channel (EC channel) whose electric field is given by the expression

$$E_k(\omega_{EC}=\omega_{C1}+\omega_{C2}-\omega_{C3}) \propto \chi^{(3)}_{klmn} E_l(\omega_{C1}) E_m(\omega_{C2}) E_n^*(\omega_{C3}), \tag{4-2}$$

where ω_i, i = EC, C1, C2 and C3, is the angular frequency of the optical wave and (*) denotes complex conjugation. $\chi^{(3)}_{klmn}$ is the third-order nonlinear susceptibility, which is a tensor of rank four and, as noted, is dependent on the states of polarization of the electric fields of C1, C2 and C3. The geometry of the FWM process considered in this work is such that the three input waves are launched into a single transverse mode waveguide (here a Semiconductor Optical Amplifier) along the same direction of propagation. The extracted product-wave hence propagates along the direction of incidence.

In a bulk SOA, the polarization dependence of the mixing product at ω_{EC} is given by

$$\hat{e}_{EC} \propto \left[(\hat{e}_{C1} \cdot \hat{e}_{C3}^{*}) \hat{e}_{C2} + (\hat{e}_{C2} \cdot \hat{e}_{C3}^{*}) \hat{e}_{C1} \right], \tag{4-3}$$

where $\hat{e}_i$, i = EC, C1, C2, and C3, is the unit vector along the direction of the electric field. This relation is strictly valid only when the unit vectors point along either the TE or TM axes of the waveguide. The terms in Equation (4-3) can be physically interpreted as the FWM signal at EC being generated as follows - C3 forms dynamic gain and index gratings with C1 (or C2). Then, C2 (or C1) scatters off this grating to generate two FWM side bands, one of them being at ω_{EC} [28]. These processes are diagrammatically represented in Figure 4.6.

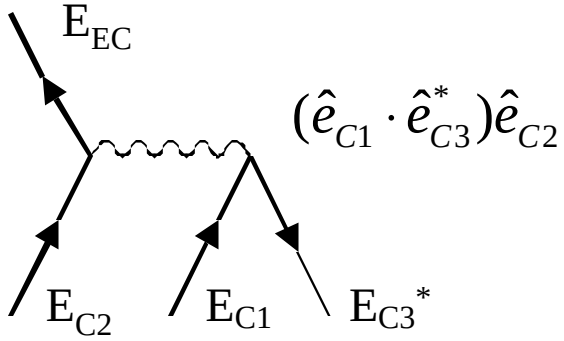

(a)

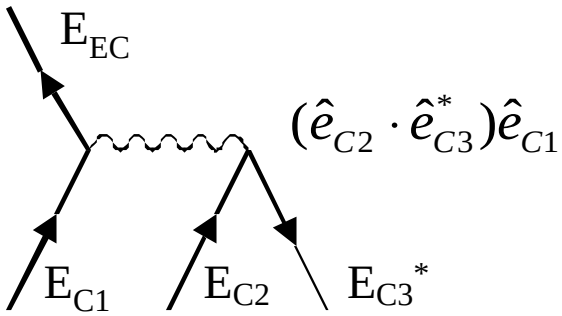

(b)

Figure 4.6: Diagrammatic representations of the non-degenerate FWM process where in (a) C3 forms a grating with C1 that scatters off C2 and in (b) C3 forms a grating with C2 that scatters off C1, to form the FWM sideband

In a Semiconductor Optical Amplifier (SOA), the unit vector $\hat{e}_i$, representing each binary state, is aligned along the TE or TM direction of the waveguide structure to avoid polarization walk-off of the incident fields arising from birefringence of the waveguide [29]. The EC signal is generated in one of the following ways:

- When all three input electric vectors are parallel (corresponding to identical bits on each channel, i.e., no errors are present), the electric field of the mixing signal at ω_{EC} is parallel to the three inputs. This is used, in turn, to generate an output when no error-correction is necessary.

- When one of the electric fields is orthogonal to the other two (corresponding to an error on that bit), a product wave at ω_{EC} is generated only when C1 and C2 are orthogonal. In this case, C3 creates a grating with either C1 or C2 (the one whose polarization is parallel to C3), which scatters energy off the third wavelength to generate a FWM signal at ω_{EC} that is orthogonal to C3. This property is utilized to correct for errors. When C3 is orthogonal to both C1 and C2, C3 cannot form a grating with either C1 or C2 and thus no mixing at ω_{EC}.

These different cases are shown in Figure 4.7,

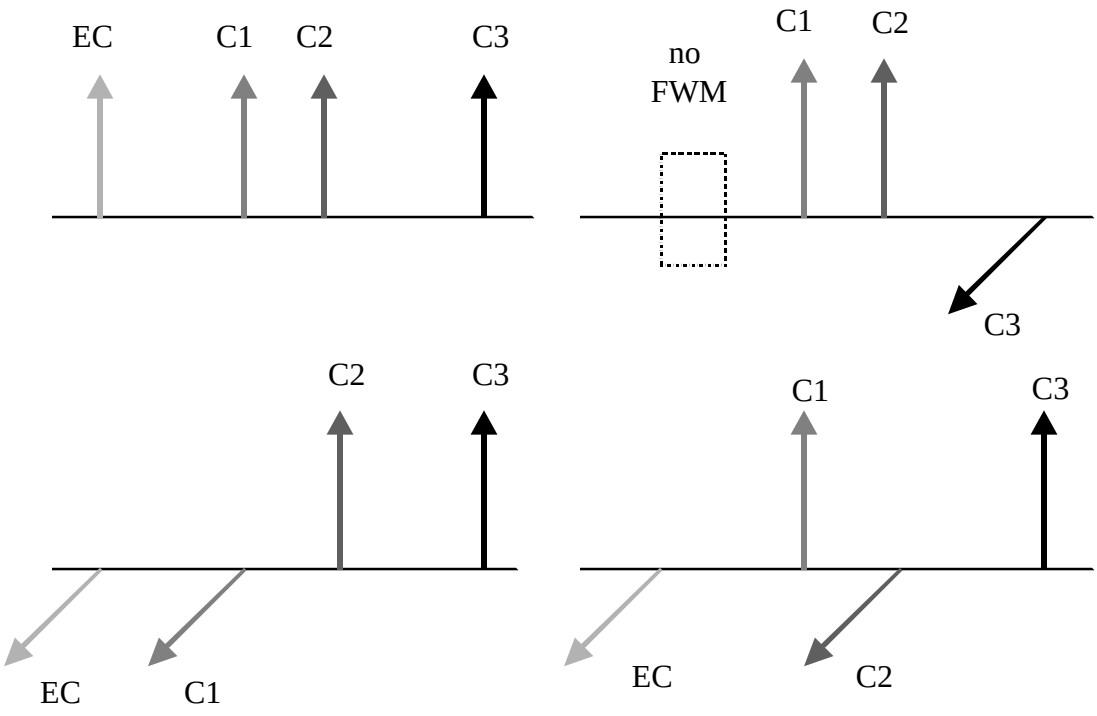

Figure 4.7: Polarization selection rules for ND-FWM between C1, C2, and C3

4.7 Error-Correcting Circuit for the (3,1) Hamming Code

The error-correcting circuit requires at least three SOAs (only two are required if retaining the PolSK format on the EC channel is not required) to generate the proper FWM signal in all possible cases. The circuit is designed in such a way that the FWM product at ω_{EC} occurs in only one SOA at a time. This is done in order to avoid interference of the desired FWM signal with additional spurious signals that would degrade the performance of the circuit. This is accomplished by adding a pre-processing element before each SOA, as shown in Figure 4.8.

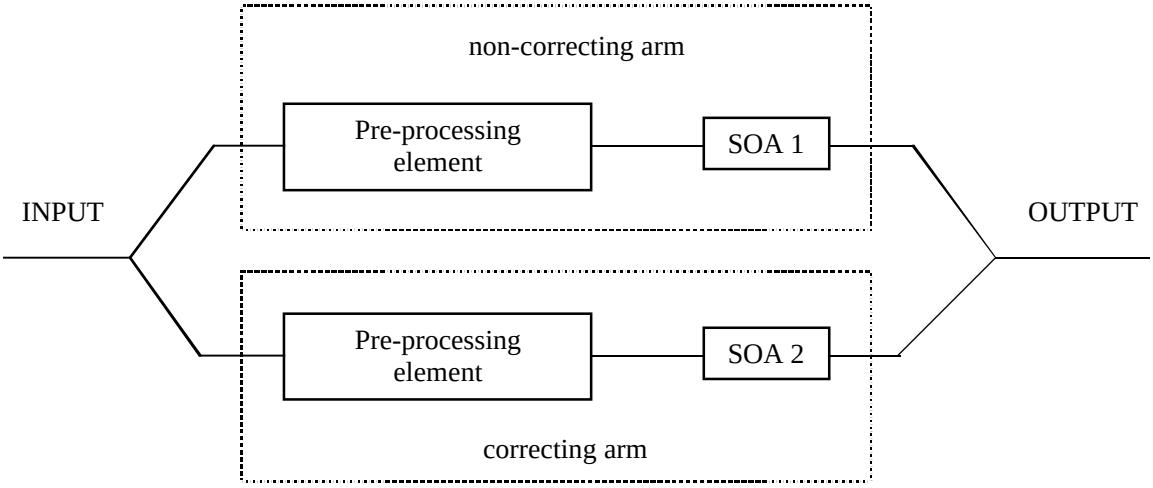

Figure 4.8: Layout of the error-correcting circuit showing the "non-correcting" and the "correcting arm"

One of the pre-processing elements is a polarizer with its transmission axis aligned to either the fast or slow axis of the polarization maintaining (PM) fiber. The other pre-processing element is a wavelength selective half-wave plate that will be referred to as the "birefringent element". It acts as a half-wave plate for C3 and a full-wave plate for C1 and C2. The result is that the state of polarization of C3 gets rotated by 90 degrees (and thus inverts the binary state on C3) while that of C1 and C2 remain almost unchanged.

The output of the circuit for each possible case is as follows:

- In the absence of any errors, C1, C2, and C3 are parallel at the input and mixing at ω_{EC} occurs in the SOA after the polarizer (SOA 1 in Figure 4.8) whose axis coincides with C1, C2, and C3. The mixing signal is parallel to the input bits and has the same binary state as the input bits. Thus the output is generated without error correction and it is for this reason that this arm is called the "non-correcting" arm. (It should be noted that a polarizer changes PolSK modulation to Amplitude Shift Keying (ASK) modulation. Hence, if PolSK modulation is to be preserved, two such non-correcting arms are required, each with a polarizer as a pre-processing element aligned to the slow and fast axes of the polarization maintaining fiber respectively.) Furthermore, when C1, C2, and C3 (all being parallel) pass through the birefringent element, which is the pre-processing element in the other arm, C3 becomes orthogonal to C1 and C2.

In this case, no mixing at ω_{EC} takes place in the SOA after the birefringent element (SOA 2 in Figure 4.8) in accordance with Equation (4-3).

- In the presence of an error, C1, C2, and C3 will not all be parallel and thus one or more of them will not pass through the polarizer. Hence no mixing will occur in SOA 1. There are two possible cases. When the error is on C3, it is orthogonal to both C1 and C2. After passing through the birefringent element, C3 will become parallel to C1 and C2 and the mixing signal in SOA 2 will have the same binary state as C1 and C2. Thus an error on C3 will be corrected. When the error is on either C1 or C2, C3 will align with the incorrect bit (since it gets inverted by the birefringent element) and will form a grating which will scatter off the correct bit to give a mixing signal parallel to the correct bit. Thus, an error-corrected signal is generated and hence the arm with the birefringent element as the pre-processing element is called the "correcting arm".

The working of the error-correcting circuit described above is shown for a few different 3-bit received Hamming words in Figure 4.9.

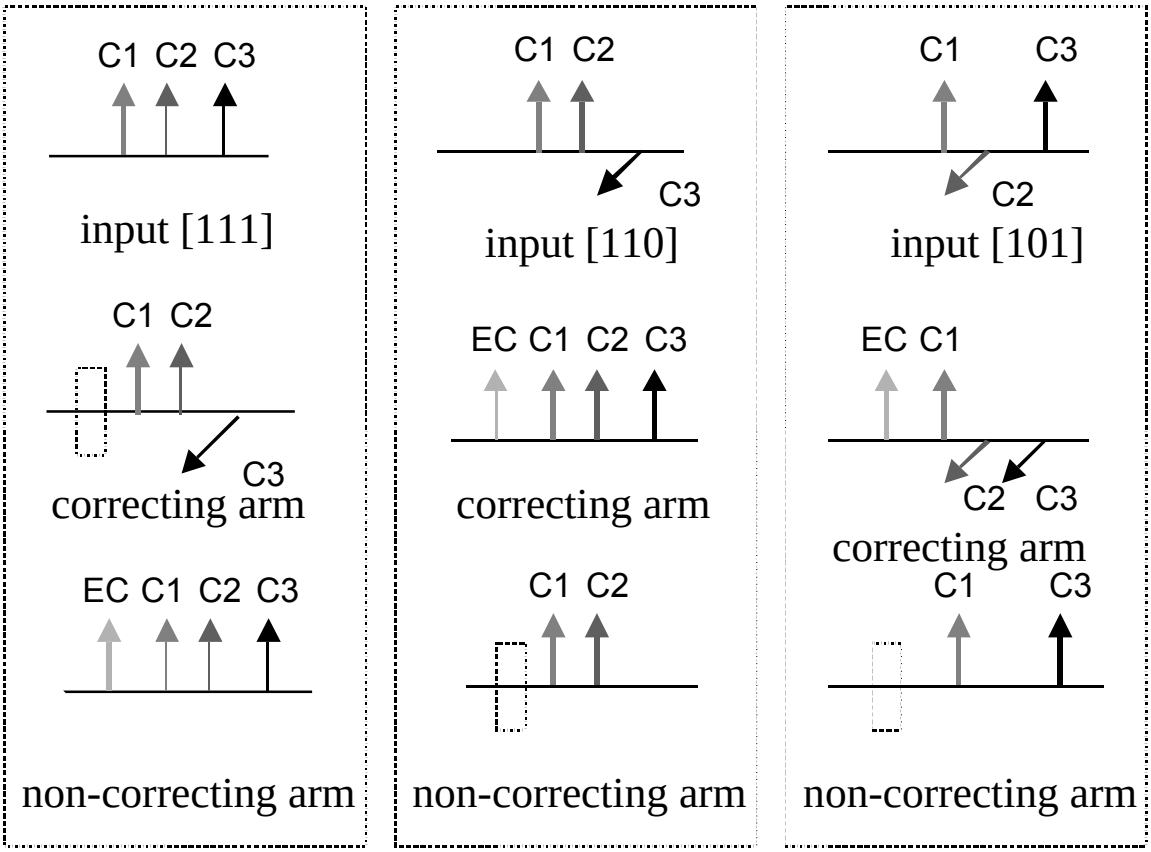

Figure 4.9: Working of the error-correcting circuit for different input Hamming words

The Boolean function corresponding to the error correction is equivalent to the computation of the "CARRY" bit of a 3-bit modulo-2 addition, can be written in terms of triple-product Boolean operations as

$$EC = (C1 \cap C2 \cap C3) \cup (\overline{C1} \cap C2 \cap C3) \cup (C1 \cap \overline{C2} \cap C3) \cup (C1 \cap C2 \cap \overline{C3}). \quad (4\text{-}4)$$

Equation (4-4) can be easily derived by noting for a general Boolean expression, "A", $\left(A \cup \overline{A}\right) = 1$. Thus each 2-bit "AND" operation in Equation (4-1) can be rewritten as

$$\left(C_i \cap C_j\right) = \left(C_i \cap C_j \cap 1\right) = C_i \cap C_j \cap \left(C_k \cup \overline{C}_k\right) = \left(C_i \cap C_j \cap C_k\right) \cup \left(C_i \cap C_j \cap \overline{C}_k\right), \tag{4-5}$$

where i, j, k = 1, 2, 3 and i≠j≠k. Adding the terms and noting that for a general Boolean expression, "A", ($A \cup A$) = A, Equation (4-4) is obtained.

It can then be seen that the Boolean operation implemented in the "non-correcting arm" is (C1∩C2∩C3), while that implemented in the "correcting arm" is ($\overline{C1}$∩C2∩C3) ∪ (C1∩$\overline{C2}$∩C3) ∪ (C1∩C2∩$\overline{C3}$). Thus each triple-product Boolean function can be associated with the terms in Equation (4-3), or a Feynman diagram shown in Figure 4.7 contributing to the FWM process.

Bibliography

1. L.A. Bergman, A.J. Mendez, and L.S. Lome, "Bit-Parallel Wavelength Links for High Performance Computer Networks," *Proc. SPIE Critical Review of Optical Science and Technology, Optoelectronic Interconnects and Packaging*, R.T. Chen and P.S. Cuilfoyle, **2R62**, 210-226 (1996).

2. N. Fujimoto, A. Ishizuka, H. Rokugawa, and K. Mori, "Skew-Free Parallel Optical Transmission Systems," *J. Lightwave Technol.*, **16**, 1822-1831 (1998).

3. Y. Ota, and R.G. Swartz, "Multi-Channel Optical Data Link (MOD-LINK)," *Proc. OEC*, **11D1-5**, 42-43 (1990).

4. M.L. Loeb, and G.R. Stilwell, Jr., "High-Speed Data Transmission on an Optical Fiber Using a Byte-Wide WDM System," *J. Lightwave Technol.*, **6**, 1306-1311 (1988).

5. A.V. Krishnamoorthy, and K.W. Goossen, "Optoelectronic-VLSI: Photonics Integrated with VLSI Circuits," *IEEE J. Sel. Top. Quant. Electron.*, **4**, 899-912 (1998).

6. S.Y. Hu, J. Ko, E.R. Hegblom, and L.A. Coldren, "Multimode WDM Optical Data Links with Monolithically Integrated Multiple-Channel VCSEL and Photodetector Arrays," *IEEE J. Quantum Elect.*, **34**, 1403-1414 (1998).

7. C.E. Zah, M.R. Amersfoort, B.N. Pathak, F.J. Favire, P.S.D. Lin, N.C. Andreadakis, A.W. Rajhel, R. Bhat, C. Caneau, M.A. Koza, and J. Gamelin, "Multiwavelength DFB Laser Arrays with Integrated Combiner and Optical Amplifier for WDM Optical Networks," *IEEE J. Sel. Top. Quant. Electron.*, **3**, 584-597 (1997).

8. M. Zirngibl, "Multifrequency Lasers and Applications in WDM Networks," *IEEE Commun. Mag.*, **36**, 39-41 (1998).

9. P. Bernasconi, C. Doerr, C. Dragone, M. Cappuzzo, E. Laskowski, and A. Paunescu, "Large N x N Waveguide Grating Routers," *J. Lightwave Technol.*, **18**, 985-991 (2000).

10. R. Adar, C.H. Henry, C. Dragone, R.C. Kistler, and M.A. Milbrodt, "Broad-band Array Multiplexers made with Silica Wave-guides on Silicon," *J. Lightwave Technol.*, **11**, 212-219 (1993).

11. E.S. Koteles, "Integrated Planar Waveguide Demultiplexers for High-Density WDM Applications," *Fiber Integrated Opt.*, **18**, 211-244 (1999).

12. M.J. Cohen, "Photodiode Arrays Help Meet Demand for WDM," *Laser Focus World*, **36**, S7–+ (2000).

13. M. Zirngibl, C.H. Joyner, and L.W. Stulz, "WDM Receiver by Monolithic Integration of an Optical Preamplifier, Wave-guide Grating Router and Photodiode-Array," *Electron. Lett.*, **31**, 581-582 (1995).

14. C.R. Doerr, M. Zirngibl, C.H. Joyner, L.W. Stulz, and H.M. Presby, "Polarization Diversity Waveguide Grating Receiver with Integrated Optical Preamplifiers," *IEEE Photonic. Tech. Lett.*, **9**, 85-87 (1997).

15. R.J. Nuyts, Y.K. Park, and P. Gallion, "Dispersion Equalization of a 10 Gb/s Repeatered Transmission System Using Dispersion Compensating Fibers," *J. Lightwave Technol.*, **15**, 31-42 (1997).

16. K.O. Hill, F. Bilodeau, B. Malo, T. Kitagawa, S. Theriault, D.C. Johnson, J. Albert, and K. Takiguchi, "Chirped in-fiber Bragg Gratings for Compensation of Optical-Fiber Dispersion," *Opt. Lett.*, **19**, 1314-1316 (1994).

17. A. Yariv, D. Fekete, and D.M. Pepper, "Compensation for Channel Dispersion by Nonlinear Optical Phase Conjugation," *Opt. Lett.*, **4**, 52-54 (1979).

18. G. Jeong, and J.W. Goodman, "Long-Distance Parallel Data Link Using WDM Transmission with Bit-Skew Compensation," *J. Lightwave Technol.*, **14**, 655-660 (1996).

19. C.C. Chen, L.A. Wang, and S.Y. Kuo, "A Wavelength Encoded Multichannel Optical Bus for Local Area Networks," *J. Lightwave Technol.*, **14**, 315-323 (1996).

20. S.K. Shao, and M.S. Kao, "WDM Coding for High-Capacity Lightwave Systems," *J. Lightwave Technol.*, **12**, 137-148 (1994).

21. S. Benedetto, and P. Poggiolini, "Theory of Polarization Shift Keying Modulation," *IEEE T. Commun.*, **40**, 708-721 (1992).

22. S. Benedetto, R. Gaudino, and P. Poggiolini, "Direct Detection of Optical Digital Transmission Based on Polarization Shift Keying Modulation," *IEEE J. Sel. Area Comm.*, **13**, 531-542 (1995).

23. R. Calvani, R. Caponi, and F. Cisternino, "Polarization Phase-Shift Keying: A Coherent Transmission Technique with Differential Heterodyne Detection," *Electron. Lett.*, **24**, 642-643 (1988).

24. E. Dietrich, B. Enning, R. Gross, and H. Knupke, "Heterodyne Transmission of a 560 Mbit/s Optical Signal by means of Polarization Shift Keying," *Electron. Lett.*, **23**, 421-422 (1987).

25. S. Benedetto, R. Gaudino, and P.Poggiolini, "Performance of Coherent Optical Polarization Shift Keying Modulation in the Presence of Phase Noise," *IEEE T. Commun.*, **43**, 1603-1612 (1995).

26. V.J. Mazurczyk, and J.L. Zyskind, "Polarization-Dependent Gain in Erbium-Doped Fiber Amplifiers," *IEEE Photonic. Tech. Lett.*, **6**, 616-618 (1994).

27. R.W. Hamming, "Error Detecting and Error Correcting Codes," *Bell Syst. Tech. J.*, **29**, 147-160 (1960).

28. G.P. Agrawal, "Population Pulsation and Nondegenerate Four-Wave Mixing in Semiconductor Laser Amplifiers," *J. Opt. Soc. Am. B*, **5**, 147-159 (1988).

29. S. Diez, C. Schmidt, R. Ludwig, H.G. Weber, P. Doussiere, and T. Ducellier, “Effect of Birefringence in a Bulk Semiconductor Optical Amplifier on Four-Wave Mixing,” *IEEE Photonic. Tech. Lett.*, **10**, 212-214 (1998).

Chapter 5

The Error-Correcting Circuit for the (3,1) Hamming Code

5.1 Introduction

The error-correcting circuit for the (3,1) Hamming Code described in the previous chapter consists of two "non-correcting arms" and one "correcting arm". Since the error-correcting circuit is a front-end device operating before photodetection, maintaining the PolSK modulation on the error-corrected (EC) channel is not required. Thus, as discussed previously, the non-correcting arm for the case when the received 3-bit word is [0,0,0] is not required. Thus the circuit consists of only one "correcting" and one "non-correcting" arm and the output on the EC channel is converted to intensity modulation before filtering the EC channel optically and detecting it with a photodetector. Details of the construction of the circuit are presented along with results of experimental demonstration.

Figure 5.1 shows the details of the experimental setup. The setup consists of three distinct parts, (i) the transmitter which generates the PolSK modulated 3-bit word, (ii) the front-end error-correcting circuit preceding the receiver, and (iii) the receiver.

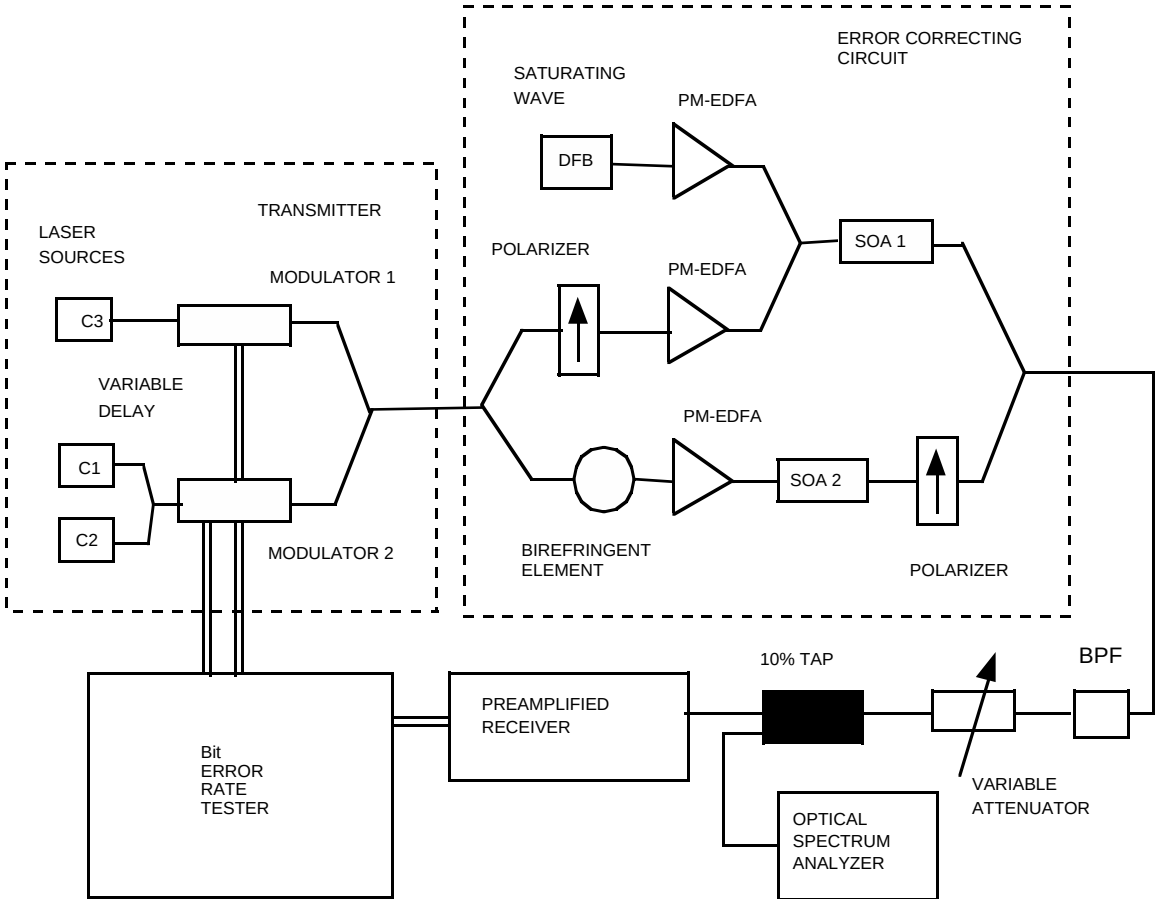

Figure 5.1: Schematic of the error-correcting circuit

The PolSK transmitter and the error-correcting circuit are built using polarization maintaining (PM) components to preserve PolSK modulation and add robustness to the setup. Besides the Optical-Signal-to-Noise (OSNR) of each channel, another important characteristic of wavelength channels is the Extinction Ratio (ER) of the States of Polarization (SOP) of the individual PolSK coded bits. The ER of a PolSK bit is defined as the ratio of the optical power present along the fast (slow) axis to the optical power present along the orthogonal axis. For power levels where OSNR of the individual channels is sufficiently high, the degradation of the ER of the PolSK bits during propagation will determine the systems performance of the error-correcting circuit. High ER of each PolSK bit must be maintained to ensure a high contrast between the "1"s and "0"s for error-free detection. In reality, perfect extinction (power is present purely along the fast or the slow axis) is not achieved. Furthermore, every PM component degrades the ER of the light that propagates through it, either due to birefringence effects or due to imperfect alignment. Thus, it is important to characterize the effect of the PM components used and the FWM process on the ER of the PolSK bits.

5.2 Characterization of the Extinction Ratio

One way to characterize each component is to measure the ER of light at the output of the PM component assuming that perfectly polarized light ($ER = \infty$) was launched at the input. This is defined as the Extinction Ratio (ER) of the PM component. The ER of a PM component indicates its ability to preserve the Extinction Ratio of the PolSK bits.

Thus the characterization of the ER of each component used or built in the setup is important.

The Extinction Ratio of a PM component can be measured using a Modular Polarization Analyzer. This instrument measures the State of Polarization (SOP) of the incident light and extracts the Stokes parameters. If $E_x e^{i\delta_x}$ and $E_y e^{i\delta_y}$ are the components of the electric field along the principal axes of a PM fiber, the Stokes parameters [1] are given as

$$s_0 = E_x^2 + E_y^2,\ s_1 = E_x^2 - E_y^2,\ s_2 = 2E_x E_y \cos\left(\delta_x - \delta_y\right),\ s_3 = 2E_x E_y \sin\left(\delta_x - \delta_y\right). \quad (6\text{-}1)$$

Since $s_0^2 = s_1^2 + s_2^2 + s_3^2$ for a well-defined SOP, the Stokes parameters can be mapped to a Poincaré sphere, where s_1, s_2 and s_3 normalized to s_0 are the spatial co-ordinates $\left(\hat{s}_1, \hat{s}_2, \hat{s}_3\right)$. For purely linear y-polarized light ($ER = \infty$), the Stokes vector is (-1, 0, 0) while for purely x-polarized light, the Stokes vector is (1, 0, 0), and the points lie on opposite ends of the equator of the Poincaré sphere. For light with a finite extinction ratio, any induced change of birefringence in the fiber (e.g., by the application of stress on the PM fiber) will change the phase factors δ_x and δ_y resulting in a change of the Stokes parameters. Thus s_0 and s_1 remain unchanged and the precession of the Stokes vector, $\left(\hat{s}_1, \hat{s}_2, \hat{s}_3\right)$, about axis $\hat{s}_1$ will form a circle with a radius R equal to $2E_x E_y / \left(E_x^2 + E_y^2\right)$. For a high extinction ratio it then follows that $R \approx 2/ER$. Thus, $ER \approx 2/R$, i.e., the ER is inversely proportional to the radius of the circle formed on the Poincaré sphere. A Polarization Analyzer deduces the ER of light after measuring the

radius of the circle that is formed on the Poincaré sphere while stress is applied to the PM fiber [2].

5.3 The PolSK Transmitter

Three New Focus external cavity tunable diode lasers are used to generate the wavelength channels for the 3-bit Hamming word. PolSK modulation is achieved by coupling the DATA and $\overline{DATA}$ outputs of a dual output Mach-Zehnder electro-optic modulator (UTP) along the fast and slow axes of a polarization maintaining fiber, using an in-fiber polarization beam combiner. Since the DATA and $\overline{DATA}$ outputs of the modulator are intensity modulated, energy is present only along the fast or the slow axis of the PM fiber. To introduce errors, one of the laser sources is connected to modulator 1, while the remaining two sources are connected to modulator 2. Non-return-to-zero (NRZ) data streams at 2.5 Gbit/s are generated using a dual output pattern generator. A variable delay line is further introduced between the pattern generator output and modulator 1 to shift the data streams temporally with respect to each other. This enables the addition of random errors on one of the bits of the 3-bit word. High ER on the PolSK bits is obtained by carefully adjusting the DC bias and the amplitude of the voltage generated from the pattern generator applied on the modulators. The values are optimized by minimizing the Bit Error Rates (BER) measured immediately after transmission. PolSK modulation is converted to Amplitude Modulation by passing the PolSK bits through an in-fiber polarizer and is detected using a high-speed photodetector. Figure 5.2 shows the PolSK transmitter.

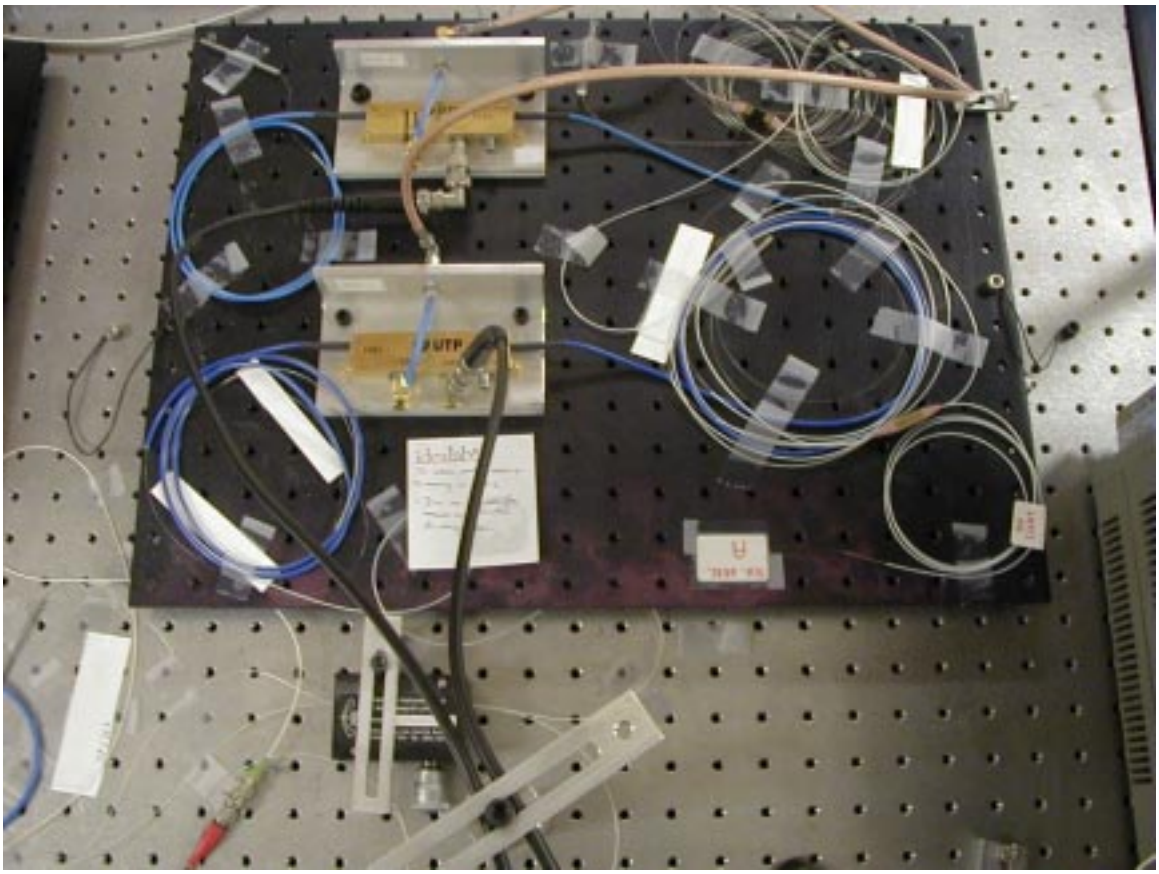

Figure 5.2: The PolSK transmitter

Figure 5.3 shows the measured Bit Error Rate (BER) versus received power for the pseudo random PolSK modulated data (2^7-1 PRBS) at 2.5 Gbit/s on channel C1.

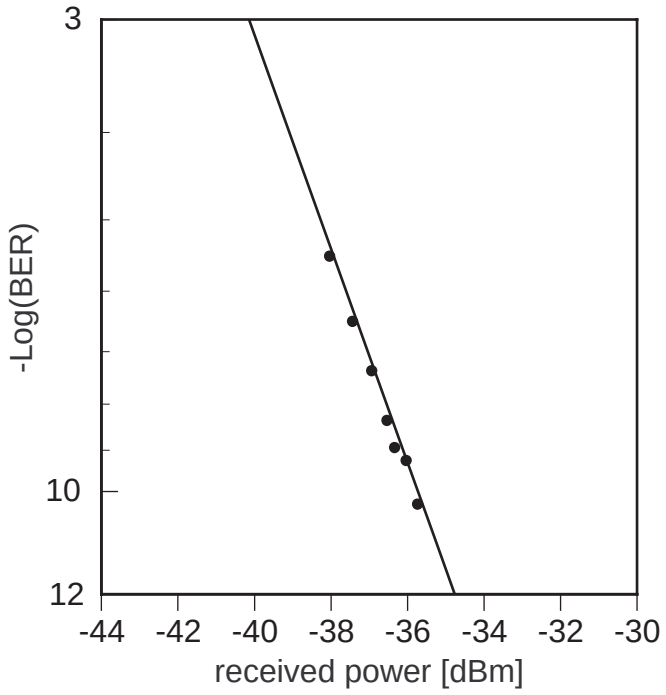

Figure 5.3: BER versus received power (in 0.5 nm Resolution Bandwidth) for PolSK modulated data at 2.5 Gbit/s measured immediately after transmission on channel C1

5.4 Building the Error-Correcting Circuit

In this section, the pre-processing elements and the Polarization Maintaining Erbium-Doped Fiber Amplifiers (PM-EDFAs) used in building the error-correcting circuit are described in detail.

A. The Pre-Processing Elements

The pre-processing element in the "non-correcting arm" is a fiber-polarizer whose axis coincides with one of the principal axes of the PM fiber. The ER of the fiber-polarizer is greater than 40 dB, or four orders of magnitude.

The pre-processing element in the "correcting arm" is a birefringent element that acts as a wavelength selective half-wave plate. The birefringent element is prepared by splicing the principal axes of a polarization maintaining Bow-tie fiber at an angle of 45 degrees on both sides with respect to the principal axes of Polarization Maintaining Panda fiber used in the rest of the setup, as shown in Figure 5.4. The length of the Bow-tie fiber is 75 cm. The birefringent element is temperature controlled to enable tunability and increased stability.

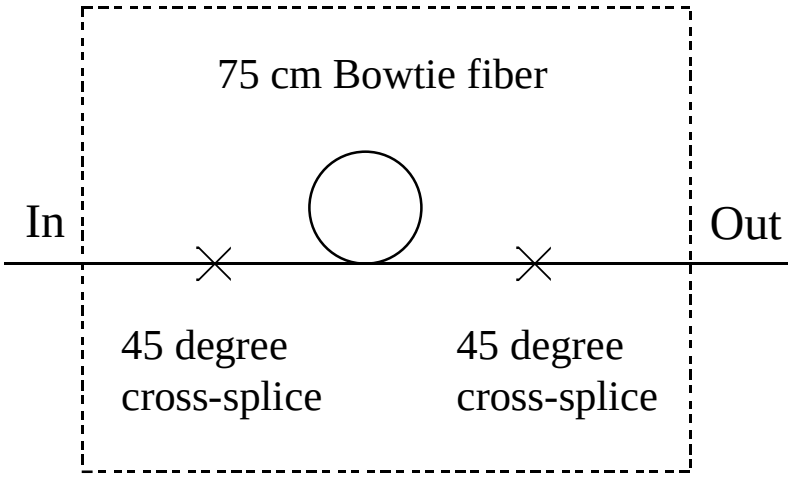

Figure 5.4: Schematic of the birefringent element

The response of the birefringent element was measured after it was inserted in the correcting arm using the setup shown in Figure 5.5. ASE from a PM-EDFA was polarized using a fiber-polarizer and launched into the correcting arm. The output of the "correcting arm" was analyzed using an Optical Spectrum Analyzer (OSA) after passing it through another fiber-polarizer. The output spectrum is shown in Figure 5.6.

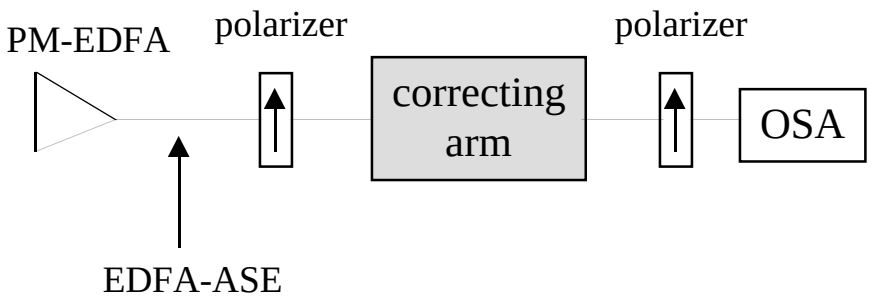

Figure 5.5: Setup to measure the response of the birefringent element

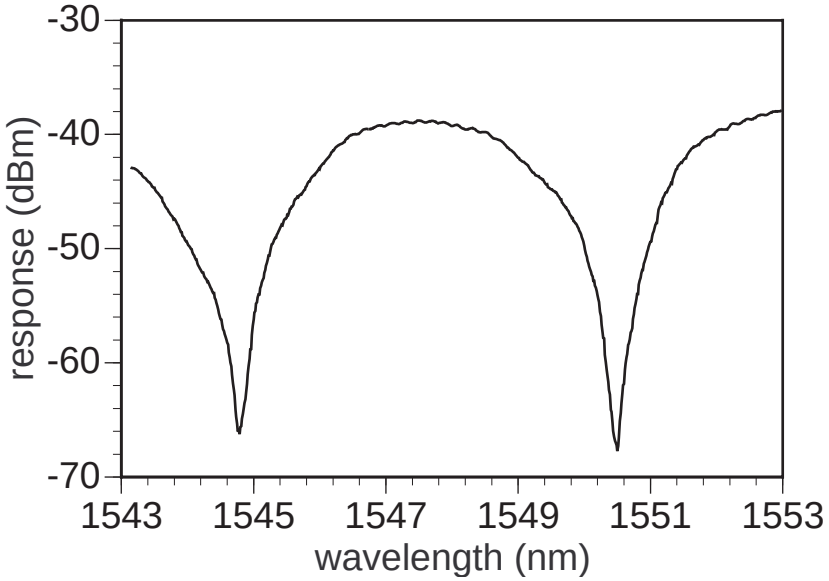

Figure 5.6: Response of the birefringent element measured by the OSA

B. Polarization Maintaining EDFA (PM-EDFA)

The PM-EDFAs used in the experiment were built with PM components using a backward pumping scheme as shown in Figure 5.7(a). Six meters of PM Erbium-doped fiber with an elliptic core from Lucent (R37PM01) was pumped with a high-power (200 mW) 1480 nm laser diode from Sumitomo. Figure 5.7(b) shows the PM-EDFA.

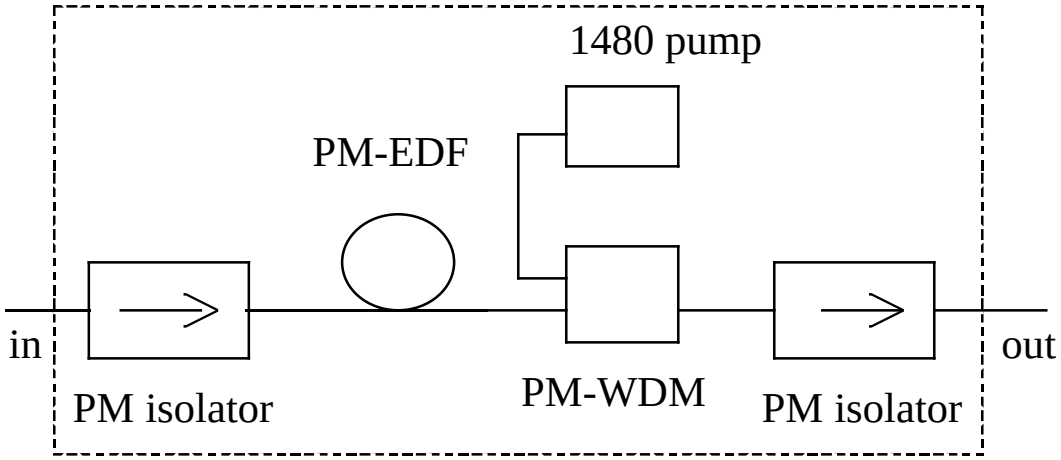

Figure 5.7(a): Schematic of the backward pumped PM-EDFA

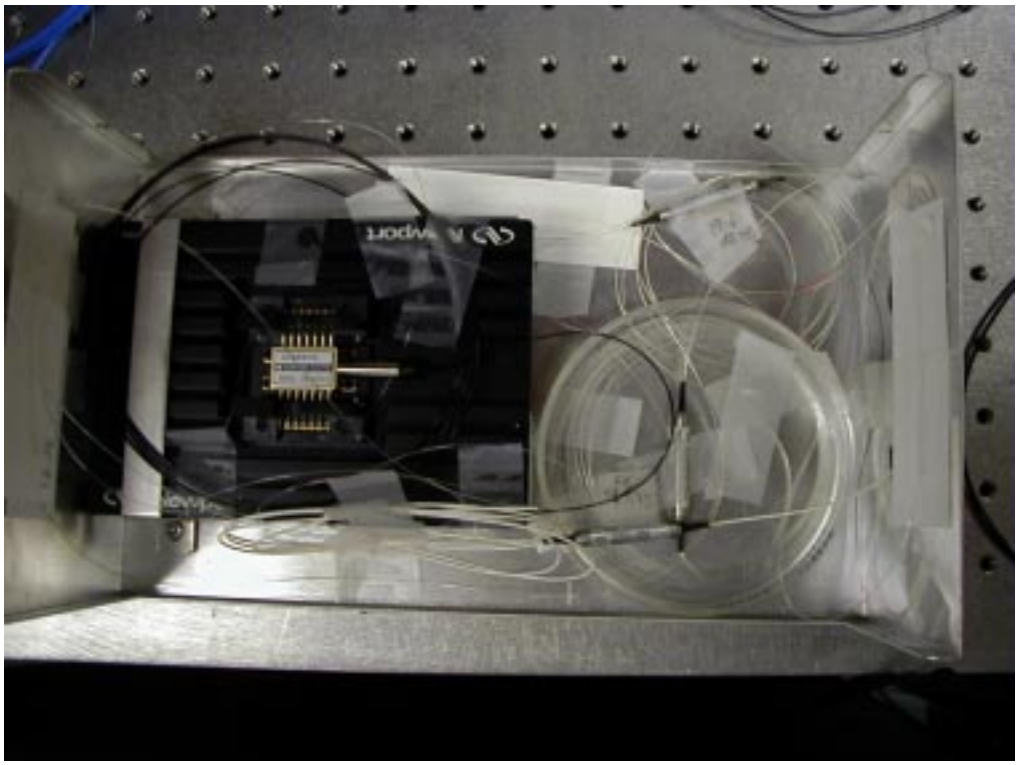

Figure 5.7(b): The PM-EDFA

The axes-alignment routines of the PM splicer (Ericsson FSU 900) could not identify the orientation of the principal axes of the PM Erbium-doped fiber. The alignment of the principal axes of the PM Erbium-doped fiber with those of the PM fiber during splicing was done manually. Linearly polarized light with high ER (>40 dB) in the Panda fiber was coupled into the PM Erbium-doped fiber pumped with the 1480 nm laser diode. The coupling was done by manually aligning the cores of the two fibers through the microscope in the splicing machine. The ER of the amplified output was analyzed on the Poincaré sphere by applying stress on the PM Erbium-doped fiber. To enable accurate measurement of the ER, the amplified output was analyzed in an optical spectrum analyzer to ensure that the ASE was suppressed and high OSNR (>40 dB in 0.1 nm Resolution Bandwidth) on the amplified signal. The PM Erbium-doped fiber was manually rotated while ensuring suppression of ASE and the ER of the amplified output was maximized by minimizing the radius of the circle on the Poincaré sphere traced by the application of stress on the fiber. The splicing procedure was repeated on the other end of the PM Erbium-doped fiber.

The ER of the PM-EDFA was then measured by launching linearly polarized light with high ER (>40 dB) and looking at the circle traced on the Poincaré sphere by applying stress on the fiber at the output of the PM-EDFA as shown in Figure 5.8(a). The result is shown in Figure 5.8(b), and ER better than 19 dB was obtained for the PM-EDFAs. Figure 5.9 shows the gain and noise figure characteristics of the PM-EDFAs measured for the 1480 nm pump laser biased at 400 mA.

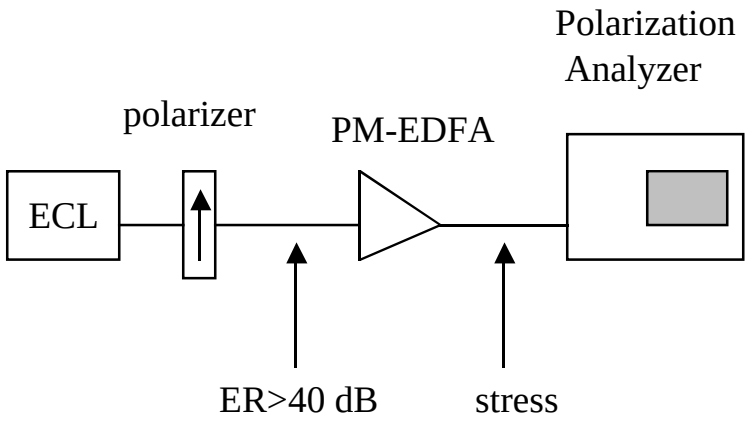

Figure 5.8(a): Setup to measure the ER of the PM-EDFA

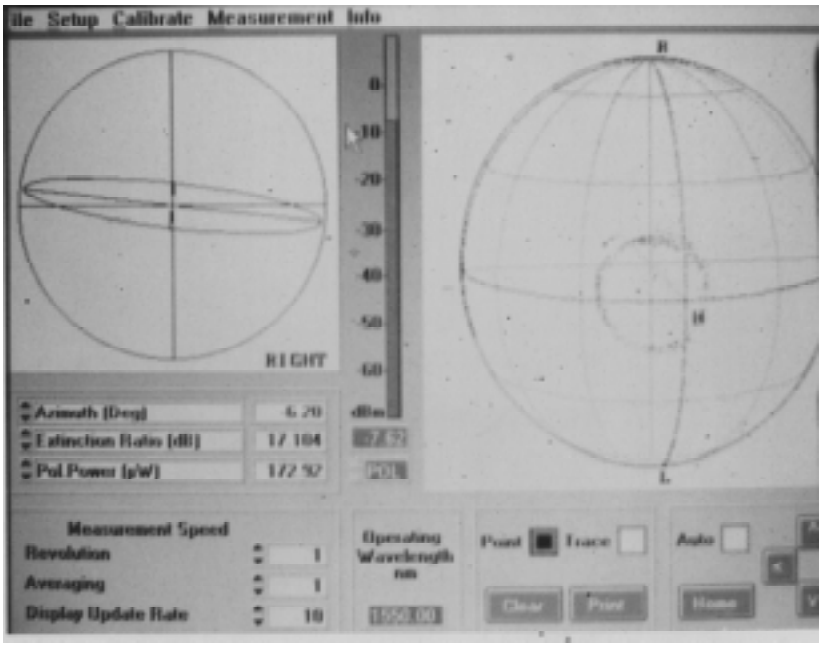

Figure 5.8(b): Circle traced on the Poincaré sphere shows 19 dB ER for PM-EDFA

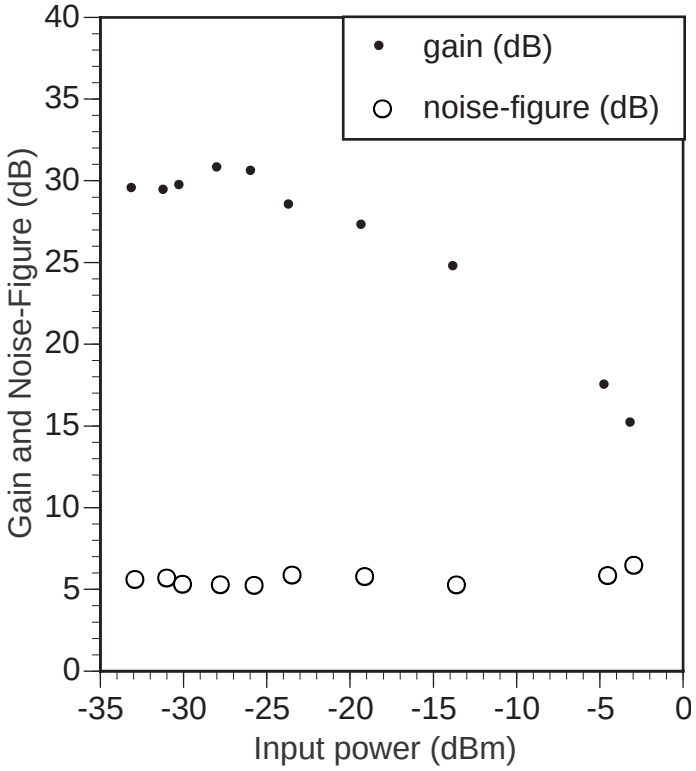

Figure 5.9: Gain and Noise Figure of the PM-EDFA

A polarizer is introduced after SOA 2 in the correcting arm to convert PolSK modulation to Amplitude Shift Keying (ASK) modulation. The lengths of the two arms in the circuit are synchronized to within 20 picoseconds, which is about 1/20-th of a bit period at 2.5 Gbit/s. This reduces undesired overlap between two temporally adjacent 3-bit words.

5.5 Experiment

The FWM process takes place in a Semiconductor Optical Amplifier (SOA) in each arm. High FWM conversion efficiency is achieved by using 1.5 mm long bulk SOAs from Optospeed biased at 650 mA. High Optical-Signal-to-Noise Ratio (OSNR) is achieved by fully saturating the SOAs after preamplifying the input channels [3] using the PM-EDFAs. The principal axes of the PM fibers are carefully aligned with the TE and TM axes of the SOA waveguide to avoid polarization walk-off of the incident fields arising from the birefringence of the waveguide [4]. The wavelengths for C1 and C2 are 1547.43 nm and 1547.85 nm (birefringent element is almost a full-wave plate) while that of C3 is 1550.47 nm (birefringent element is a half-wave plate). Note that the SOA in the correcting arm is always saturated since there is always power incident on it. However, the SOA in the non-correcting arm is not saturated when all the bits are identically "0", as the polarizer before it does not allow any channel to pass through and be amplified. This leads to a modulation of Amplified Spontaneous Emission (ASE) from SOA 1, because its gain recovery time is comparable to the bit rate. Thus an additional CW laser is coupled into SOA 1, which is called the "saturating-wave laser" (see Figure 5.1). Its power is adjusted such that it is low compared to the power in the other channels, but high enough to ensure saturation of SOA 1. Its wavelength is carefully selected at 1558.5 nm so that the additional FWM sidebands that it generates do not interfere with the EC channel. Figure 5.10 shows the optical spectrum at the output of SOA 1 (in 0.1 nm Resolution Bandwidth) when the 3-bit word is [1,1,1]. The wavelength channels C1, C2, and C3 along with the desired FWM process at ω_{EC} are marked in the spectrum.

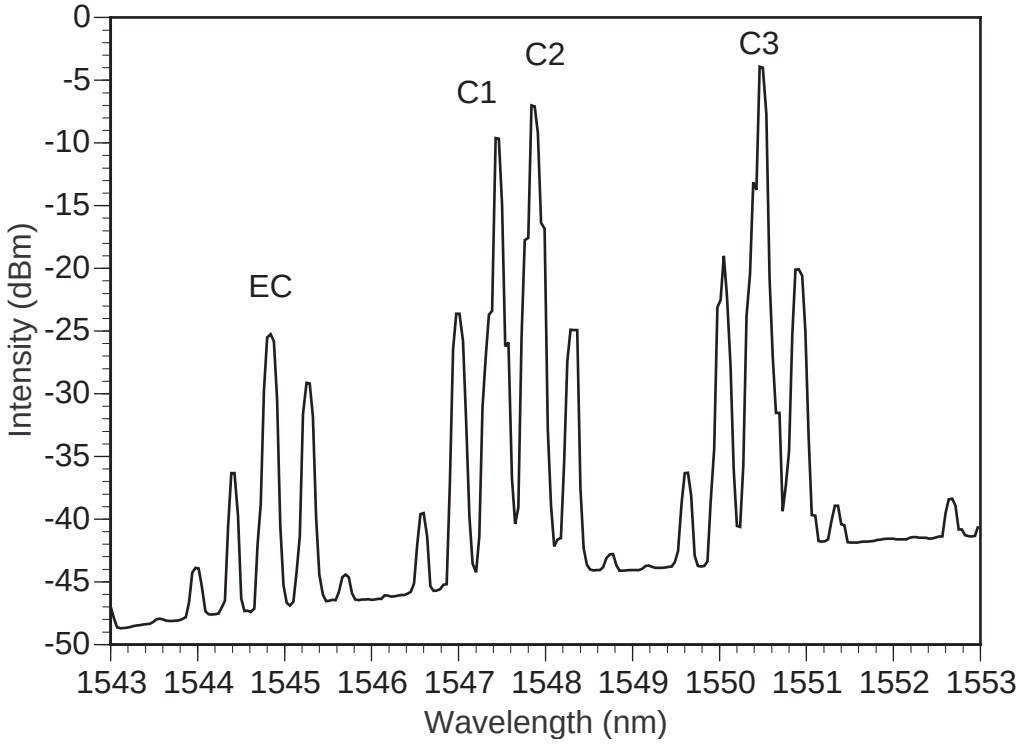

Figure 5.10: Optical spectrum at the output of the SOA (in 0.1 nm Resolution Bandwidth) showing the wavelengths channels [C1-C3] and EC (from Ref. [7])

The SOAs are further tested for mode conversion effects [5], which would lead to a degradation of the extinction ratio of the PolSK signals. TE polarized light is launched into the SOAs operating under identical conditions as used in the experiment. Using another polarizer at the output of the SOAs, the TM component is found to be at least 30 dB lower than the TE component, which is of the same order as the extinction ratio of the polarizers used in the measurement. For TM polarized light launched into the SOAs, the TE component at the output is also found to be at least 30 dB lower than the TM

component. Hence, we conclude that mode conversion is not significant in the devices used in this experiment.

The output from each arm is combined using a polarization maintaining coupler. Spurious interference can occur between the two arms due to the presence of power in the EC channel originating in the arm where FWM is not supposed to occur. This is because the state of polarization on each channel is not perfectly linear along the fast or the slow axis of the PM fiber, leading to a residual power in the orthogonal direction. This interference is minimized by coupling the EC channel in each arm to the orthogonal axes of the PM fiber. The error-corrected channel is filtered and detected using a pre-amplified receiver. The "correcting arm" of the error-correcting circuit is shown in Figure 5.11.

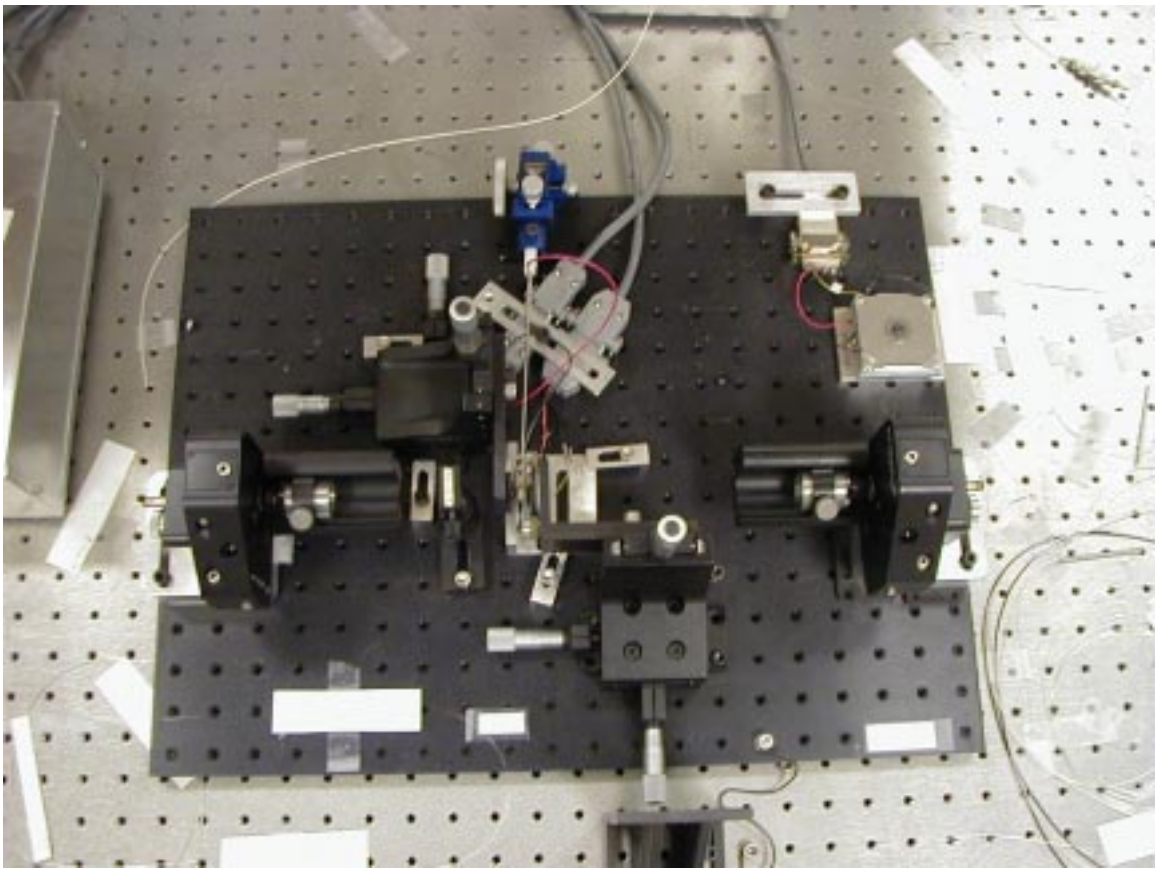

Figure 5.11: The “correcting arm” of the error-correcting circuit

5.6 Results and Discussions

The performance of error-correcting circuit was first tested with CW waves to evaluate the ability of the components to control and preserve the States of Polarization (SOP) on the three channels C1, C2, and C3. The SOP of each channel was adjusted by changing the DC bias on the Mach-Zehnder modulators and the FWM signal generated in each SOA of the "non-correcting arm" and the "correcting arm". Figure 5.12 shows the optical

spectra obtained when the 3-bit word was adjusted to be [1,1,1]. Figure 5.12(a) shows the FWM signal generated in the "non-correcting arm" while Figure 5.12(b) shows the FWM signal generated in the "correcting arm".

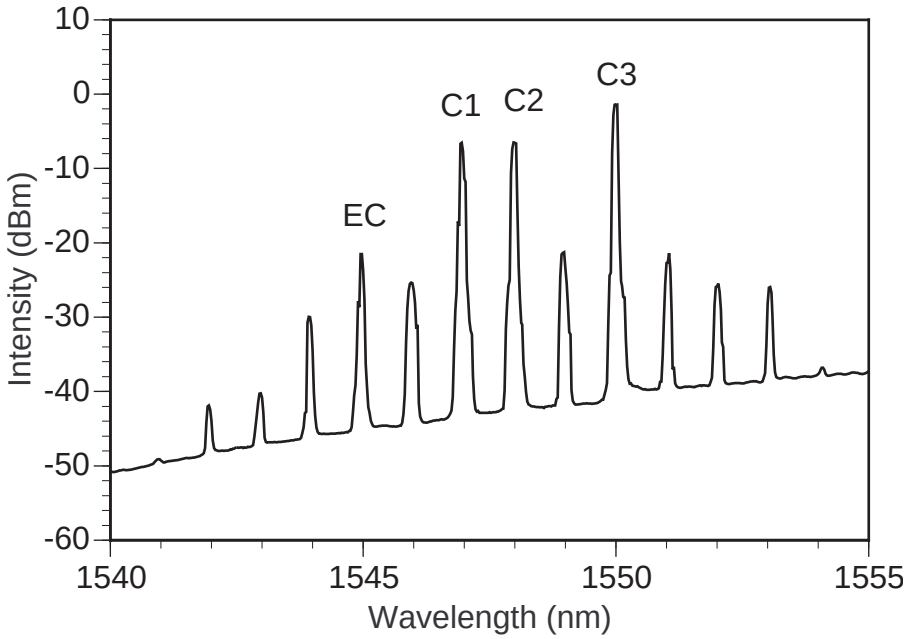

Figure 5.12(a): Optical Spectrum after the SOA (in 0.1 nm Resolution Bandwidth) in the "non-correcting arm" for the received word [1,1,1] (after Ref. [6])

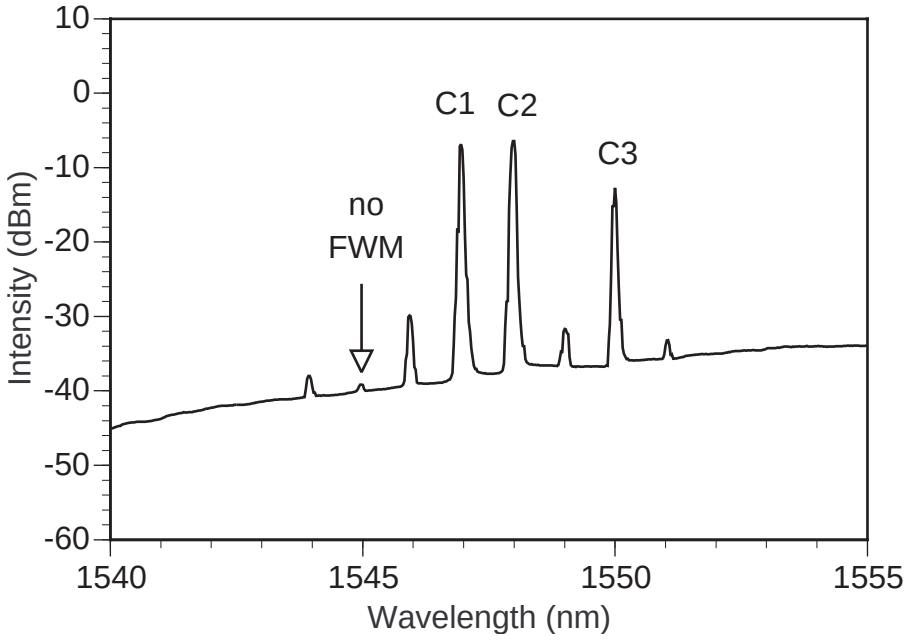

Figure 5.12(b): Optical Spectrum after the SOA (in 0.1 nm Resolution Bandwidth) in the "correcting arm" for the received word [1,1,1] (after Ref. [6])

The results of Figure 5.12 show a good amplitude Extinction Ratio (~20 dB) on the FWM signal generated in the two arms for the input word being [1,1,1]. Dynamic performance of the error-correcting circuit was tested at 2.5 Gbit/s. Figure 5.13(a) shows an 8-bit pattern [10011100] that was encoded on channels C1 and C2 using modulator 1 (see Figure 5.1). The encoded information on channel C3 was inverted by adjusting the DC bias on modulator 2 and the 8-bit pattern on C3 is shown in Figure 5.13(b). Thus the data encoded on channel C3 is always erroneous with respect to the data on channels C1 and C2. The 8-bit pattern recovered on the FWM signal after combining the "non-

correcting arm" and the "correcting arm" is shown in Figure 5.13(c) and it corresponds to the pattern on channels C1 and C2. Hence the information coded on the 3-bit Hamming word is corrected for single errors.

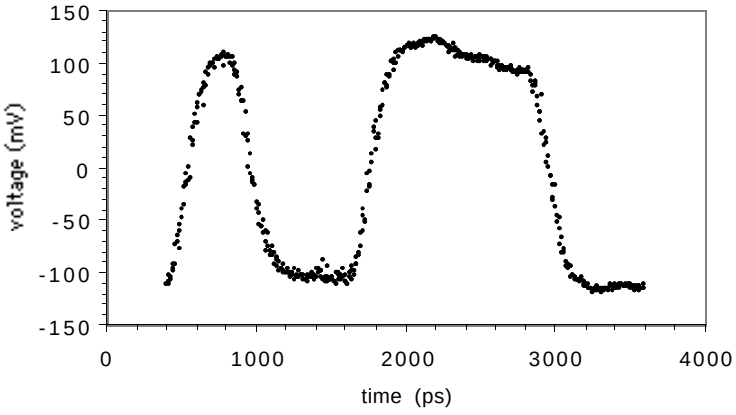

(a)

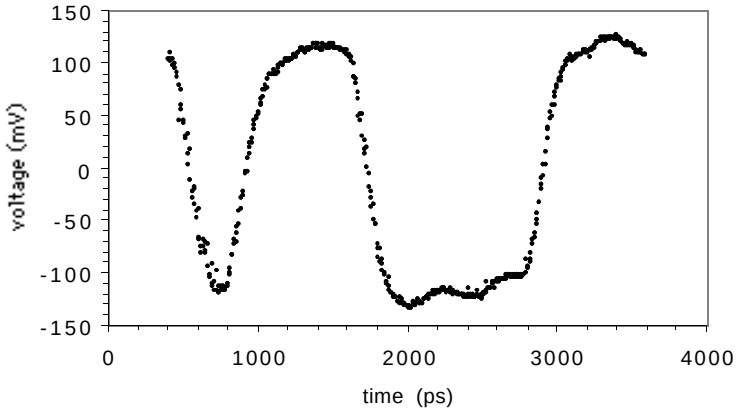

(b)

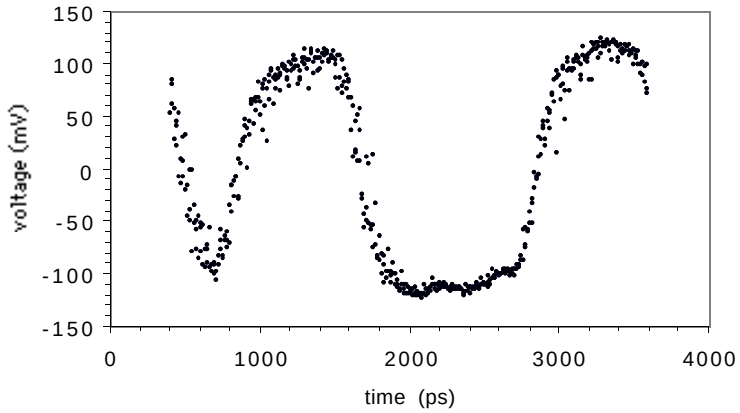

(c)

Figure 5.13: Oscilloscope traces of the 8-bit pattern for (a) erroneous data on channel C3, (b) data on channels C1 and C2, and (c) error-corrected FWM signal (from Ref. [6])

Figure 5.14(a) shows a 16-bit pattern [1001110011110000] at 2.5 Gbit/s on each channel. The variable time delay is adjusted so that there is a one-bit delay on C3 relative to C1 and C2. Thus, C3 is the channel which has occasional errors. The resultant patterns on ω_{EC}, which are obtained from the non-correcting and correcting arm separately, are shown in Figure 5.14(b) and 5.14(c), respectively. Figure 5.14(d) shows the pattern on ω_{EC} after both arms have been combined which is identical to the pattern on C1 and C2. This shows that the data stream with errors was corrected.

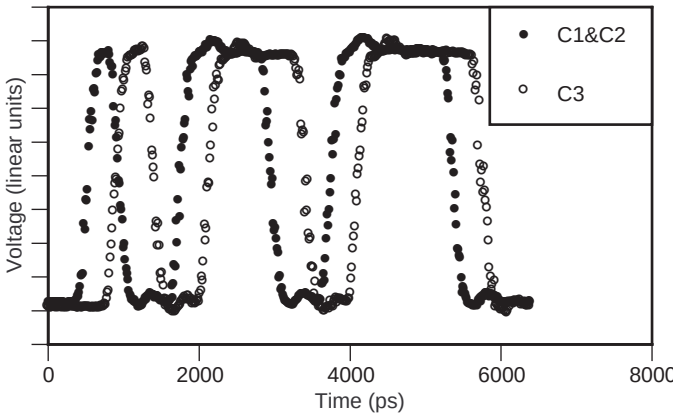
C1&C2
C3
Voltage (linear units)
0
2000
4000
6000
8000
Time (ps)

(a)

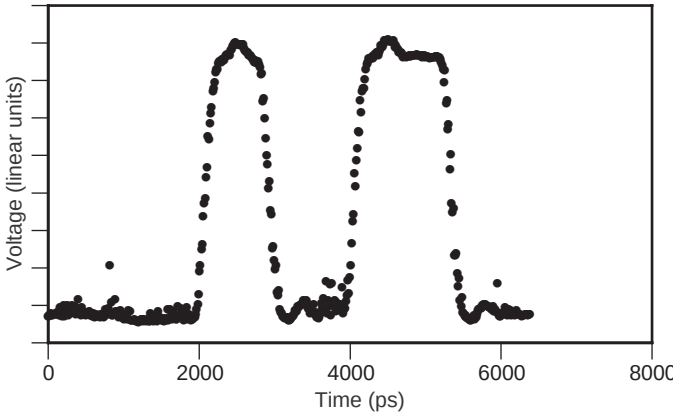
Voltage (linear units)
0
2000
4000
6000
8000
Time (ps)

(b)

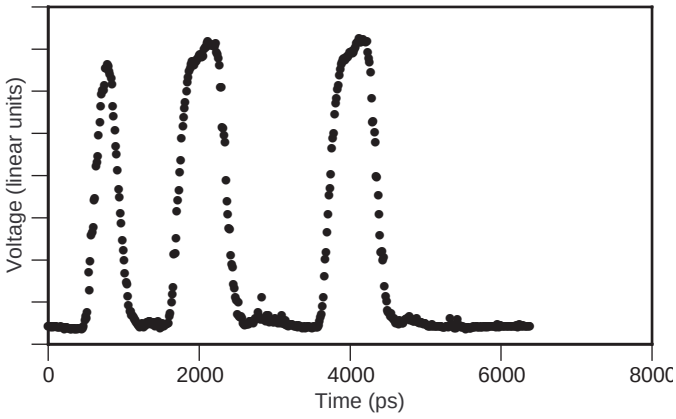
Voltage (linear units)
0
2000
4000
6000
8000
Time (ps)

(c)

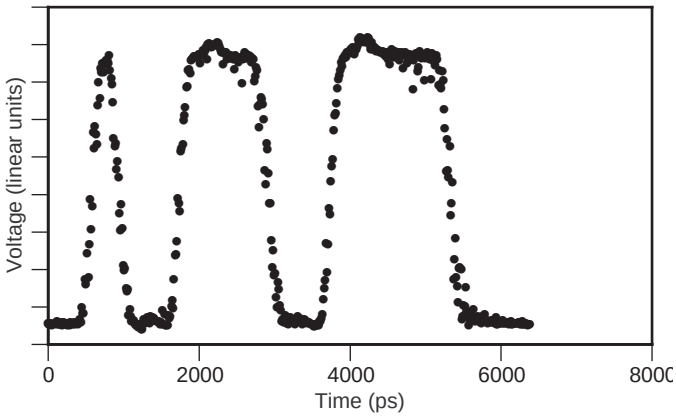

(d)

Figure 5.14: Oscilloscope traces of (a) 16-bit patterns on channels C1, C2, and C3 at 2.5 Gbit/s, (b) EC output from the non-correcting arm, (c) EC output from the correcting arm, and (d) EC output from both arms combined (from Ref. [7])

We further demonstrate the dynamic operation of this circuit by modulating C1, C2, and C3 with a pseudo-random bit stream (2^7-1 PRBS), with a one bit delay on C3 relative to C1 and C2. In this case the binary state on C3 is complementary to the state on C1 and C2 approximately 50 percent of the time. Figure 5.15(a) shows the Bit Error Rate (BER) versus received power (in 0.5 nm Resolution Bandwidth) of the EC channel for this case. This is compared to the case when there is no errors on C3 relative to C1 and C2. Detection with a low Bit Error Rate $<10^{-9}$ is demonstrated despite a 50 percent error rate on the received word. Similar results are obtained by modulating C1, C2 and C3 with pseudo-random bit streams with a one bit delay on C1 relative to C3 and C2, in which case the binary state on C1 is complementary to that on C2 and C3 approximately 50

percent of the time. The Bit Error Rate for this is shown in Figure 5.15(b). The slight degradation after error correction in Figure 5.15(b) compared to Figure 5.15(a) can be explained by the lowering of FWM efficiency in the correcting arm when C1 and C2 are orthogonal compared to when C1 and C2 are parallel, as determined by Equation (4-3). Figure 5.16 shows the eye diagram obtained on the EC channel after error correction.

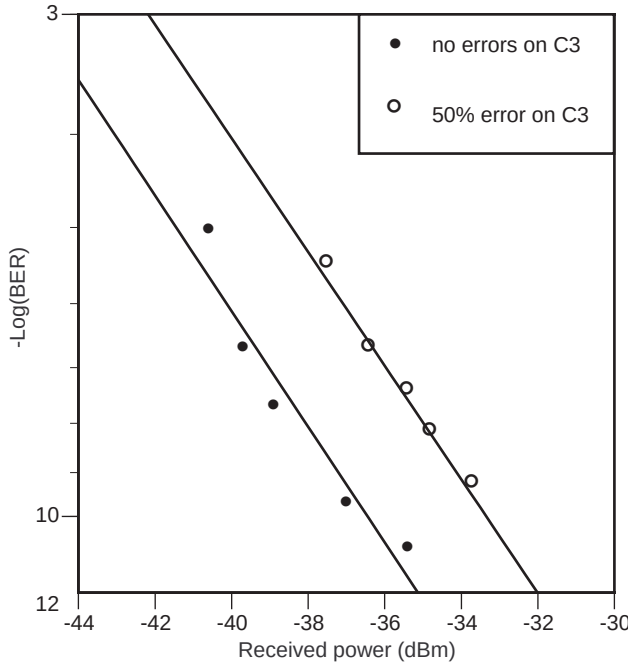

Figure 5.15(a): BER versus received power (in 0.5 nm Resolution Bandwidth) at 2.5 Gbit/s for random errors on C3 (from Ref. [7])

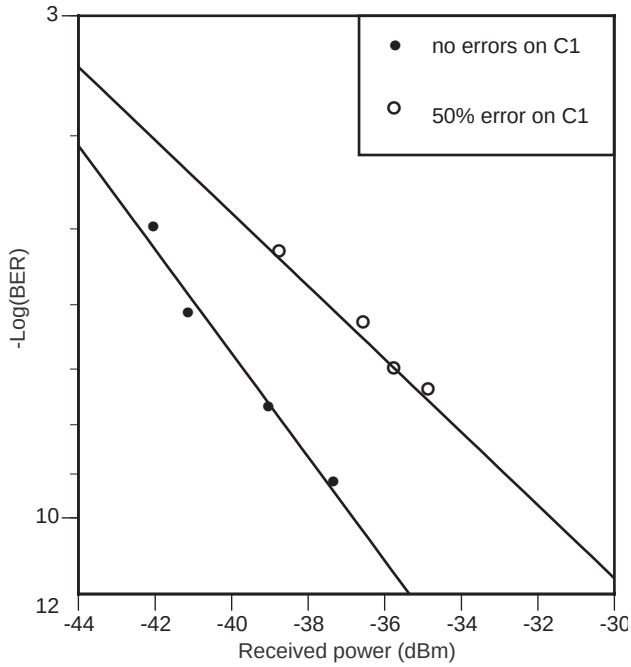

Figure 5.15(b): BER versus received power (in 0.5 nm Resolution Bandwidth) at 2.5 Gbit/s for random errors on C1 (from Ref. [7])

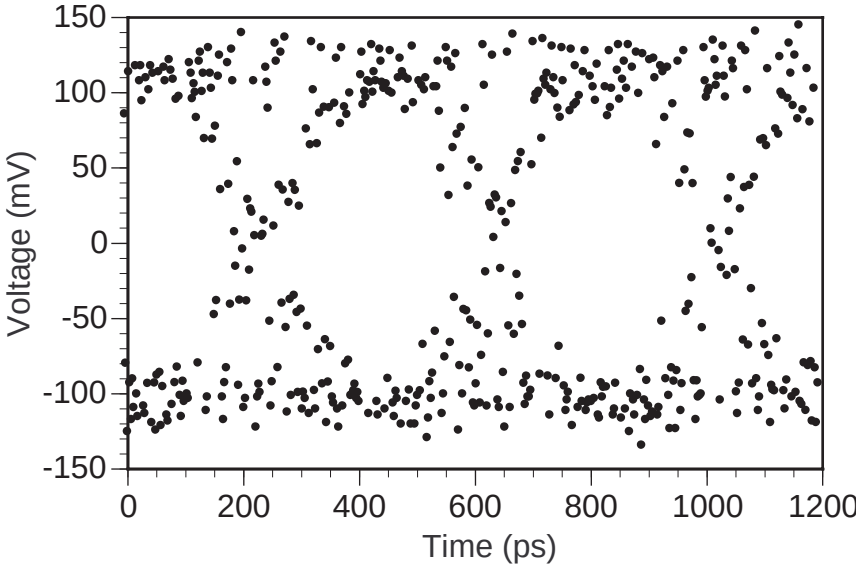

Figure 5.16: Eye diagram after error-correction on the EC channel

The operation of the logic circuit is further tested when the information on C3 is severely distorted, so that a Bit Error Rate no better than 30 percent could be achieved on C3. This is achieved by changing the DC-bias of the Mach-Zehnder modulator. Thus the information on C3 is ambiguous in that there are no clearly defined binary states on it. Pseudo-random bit streams on C1 and C2 were detected to be error-free upon transmission through the circuit. Figure 5.17 shows the Bit Error Rate versus received power on the EC signal for this case. Once again a low Bit Error Rate $<10^{-9}$ on the mixing signal for ambiguous data on C3 and error-free data on C1 and C2 is demonstrated. This shows that error-correction on certain ill-defined states is also possible.

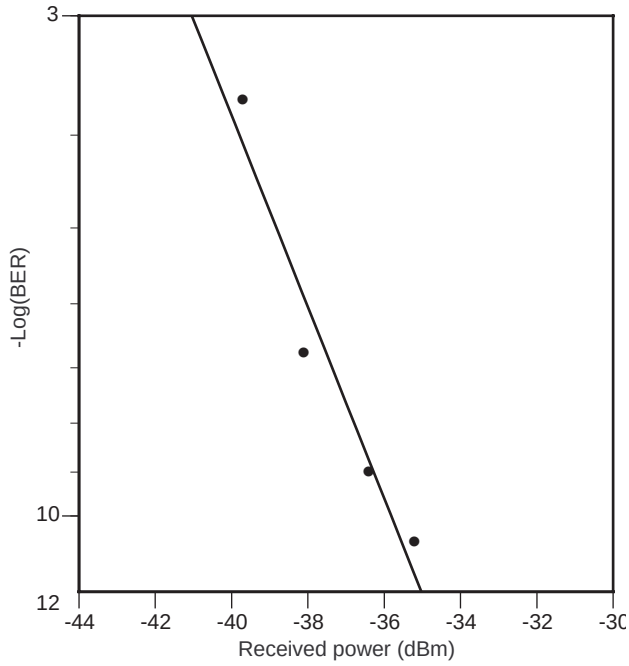

Figure 5.17: BER versus received power (in 0.5 nm Resolution Bandwidth) at 2.5 Gbit/s for error correction on ill-defined states with 30% errors on C3 (from Ref. [7])

Bibliography

1. J.D. Jackson, *Classical Electrodynamics*, John Wiley & Sons, New York, NY, 1998.

2. "Modular Polarization Measurement System, PAT 9000," Operation Manual, Profile Optische Systeme GmbH, 1998.

3. A. D'Ottavi, P. Spano, G. Hunziker, R. Paiella, R. Dall' Ara, G. Guekos, and K.J. Vahala, "Wavelength Conversion at 10 Gb/s by Four-Wave Mixing Over a 30-nm Interval," *IEEE Photonic. Tech. Lett.*, **10**, 952-954 (1998).

4. S. Diez, C. Schmidt, R. Ludwig, H.G. Weber, P. Doussiere, and T. Ducellier, "Effect of Birefringence in a Bulk Semiconductor Optical Amplifier on Four-Wave Mixing," *IEEE Photonic. Tech. Lett.*, **10**, 212-214 (1998).

5. H. Soto, D. Erasme, and G. Guekos, "Cross-Polarization Modulation in Semiconductor Optical Amplifiers," *IEEE Photonic. Tech. Lett.*, **11,** 970-972 (1999).

6. A. Bhardwaj, P.O. Hedekvist, H. Andersson, and K.J. Vahala, "All Optical Front End Error Correction on a Spectral Data Bus," Paper CWI5, presented at the *Conference on Lasers and Electro-Optics*, San Francisco, CA, May 7-12 (2000).

7. A. Bhardwaj, P.O. Hedekvist, and K. Vahala, "All-Optical Logic Circuits Based on Polarization Properties of Nondegenerate Four-Wave Mixing," *J. Opt. Soc. Am. B*, **18**, 657-665 (2001).

Chapter 6

All-Optical Logic Circuits Based on Polarization Properties of ND-FWM

6.1 Introduction

The error-correcting circuit for the (3,1) Hamming code based on the polarization properties of ND-FWM can be further generalized to implement other Boolean functions, such as a 3-bit addition. The scheme can also be used to implement more than one Boolean operation simultaneously in the same set of SOAs using different ND-FWM processes. Higher level Hamming codes can be implemented using the 3-bit adder circuits as fundamental building blocks and it will be seen that the circuit design for the (7,4) Hamming Code exhibits the symmetries of the error-correcting code. Pertinent issues such as the cascading of such circuits and degradation of the Extinction Ratio (ER) of the PolSK coded bits after each cascade, are investigated further.

6.2 Generalization to a 3-bit Adder

The Boolean function for error correction using the (3,1) Hamming code on the 3-bit word [C1, C2, C3] is identical to computing the "CARRY" bit of the modulo-2 3-bit addition of the bits C1, C2 and C3. If CARRY[C1, C2, C3] and SUM[C1, C2, C3] denote the "CARRY" and "SUM" bits of the modulo-2 3-bit addition of C1, C2 and C3,

$$CARRY[C1, C2, C3] = (C1 \cap C2) \cup (C2 \cap C3) \cup (C1 \cap C3) \tag{6-1}$$

$$SUM[C1, C2, C3] = C1 \oplus C2 \oplus C3, \tag{6-2}$$

where "$\cup$" denotes the Boolean "OR" function, "$\cap$" denotes the Boolean "AND" function and "$\oplus$" denotes the Boolean function Exclusive-OR (XOR). The "SUM" bit can be written in terms of the triple product Boolean functions using the identities, $(A \oplus B) = \left(A \cap \overline{B}\right) \cup \left(\overline{A} \cap B\right)$, $\left(\overline{A \cap B}\right) = \overline{A} \cup \overline{B}$, $\left(\overline{A \cup B}\right) = \overline{A} \cap \overline{B}$ and $\left(A \cap \overline{A}\right) = 0$. Thus,

$$\text{SUM} = (\text{C1} \cap \text{C2} \cap \text{C3}) \cup (\text{C1} \cap \overline{C2} \cap \overline{C3}) \cup (\overline{C1} \cap \text{C2} \cap \overline{C3}) \cup (\overline{C1} \cap \overline{C2} \cap \text{C3}). \tag{6-3}$$

In comparision, the "CARRY" bit is given by Equation (4-4) as

$$\text{CARRY} = (\text{C1} \cap \text{C2} \cap \text{C3}) \cup (\overline{C1} \cap \text{C2} \cap \text{C3}) \cup (\text{C1} \cap \overline{C2} \cap \text{C3}) \cup (\text{C1} \cap \text{C2} \cap \overline{C3}). \tag{6-4}$$

The "CARRY" bit was implemented using the error correcting circuit, where the first term on the right hand side was generated in the "non-correcting arm" and the remaining three terms were generated in the "correcting arm" of the circuit. The "SUM" bit operation can also be implemented by inverting the output of the "correcting arm" in the circuit, i.e., using a "NOT" function in the "correcting arm" before combining it with the "non-correcting arm". With PM fiber, the NOT function can be implemented with the use of a 90 degree cross-splice between the principal axes of two PM fibers.

Figure 6.1 shows how the "SUM" and "CARRY" bits of the 3-bit addition can be generated in the same set of SOAs. Thus it is possible to implement two different truth tables related to the modulo-2 3-bit addition in the same circuit.

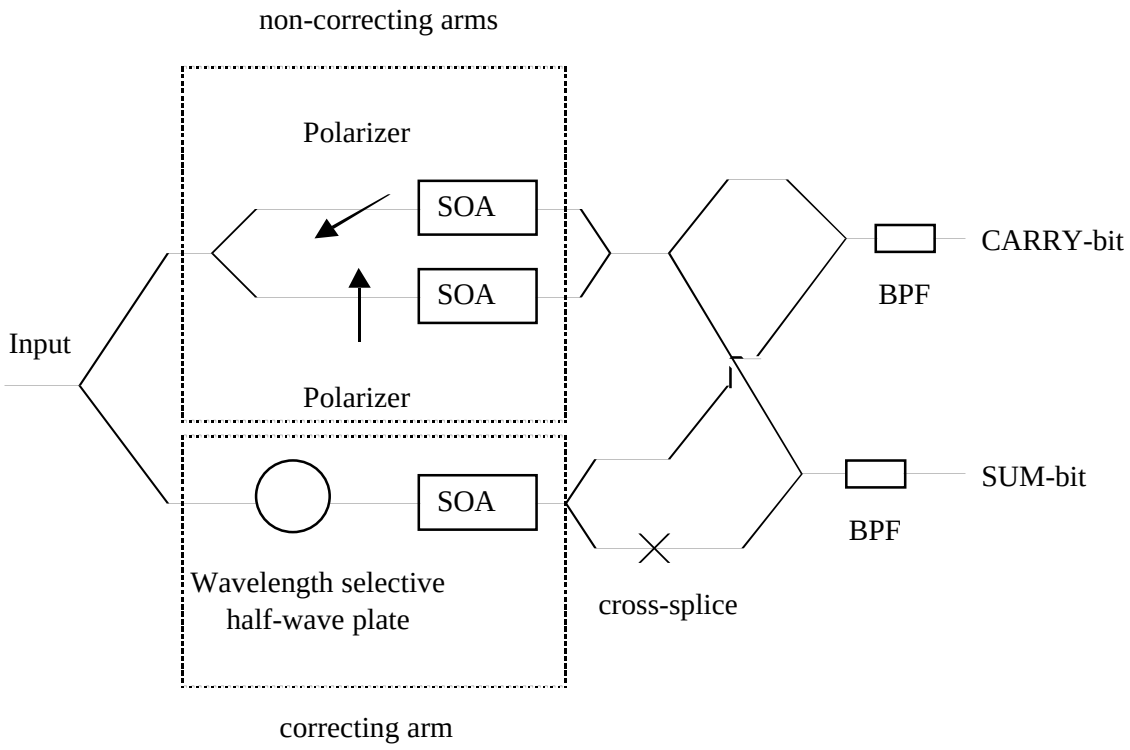

Figure 6.1: Schematic of the full 3-bit adder (from Ref. [2])

6.3 Encoding the (7,4) Hamming Code

The (3,1) Hamming Code has a high overhead due to the high redundancy. This overhead can be reduced by the use of more sophisticated error correcting codes [1] and the study of these codes has been an area of active research. The (7,4) Hamming Code is the next higher-level Hamming Code with a lower redundancy than the (3,1) Hamming Code. The "SUM" bit, C1 ⊕ C2 ⊕ C3, also corresponds to the parity of the three bits C1, C2, and C3 and can be used to generate parity bits for encoding of other Hamming Codes.

For example, the encoder for the (7,4) Hamming Code takes four input data bits [D1, D2, D3, D4] and creates three additional parity bits given by

$$P\text{-}(412) = D4 \oplus D1 \oplus D2 \tag{6-5a}$$

$$P\text{-}(423) = D4 \oplus D2 \oplus D3 \tag{6-5b}$$

$$P\text{-}(413) = D4 \oplus D1 \oplus D3, \tag{6-5c}$$

i.e., the parity bits are “SUM” bits of the 3-bit additions of D4 with two additional bits $[D_i, D_k]$ (i,k=1,2,3) from the remaining three bits (there is nothing special about D4, it is just taken for this example). For spectrally placed channels [D1-D4], each ND-FWM of D4 with $[D_i, D_k]$ will occur at a different wavelength channel as shown experimentally in Figure 6.2 and given by

$$E_k(\omega_{P\text{-}(412)}=\omega_{D1}+\omega_{D2}-\omega_{D4}) \propto \chi^{(3)}_{klmn} E_l(\omega_{D1})E_m(\omega_{D2})E_n^*(\omega_{D4}) \quad (6\text{-}6a)$$

$$E_k(\omega_{P\text{-}(423)}=\omega_{D2}+\omega_{D3}-\omega_{D4}) \propto \chi^{(3)}_{klmn} E_l(\omega_{D2})E_m(\omega_{D3})E_n^*(\omega_{D4}) \quad (6\text{-}6b)$$

$$E_k(\omega_{P\text{-}(413)}=\omega_{D1}+\omega_{D3}-\omega_{D4}) \propto \chi^{(3)}_{klmn} E_l(\omega_{D1})E_m(\omega_{D3})E_n^*(\omega_{D4}). \quad (6\text{-}6c)$$

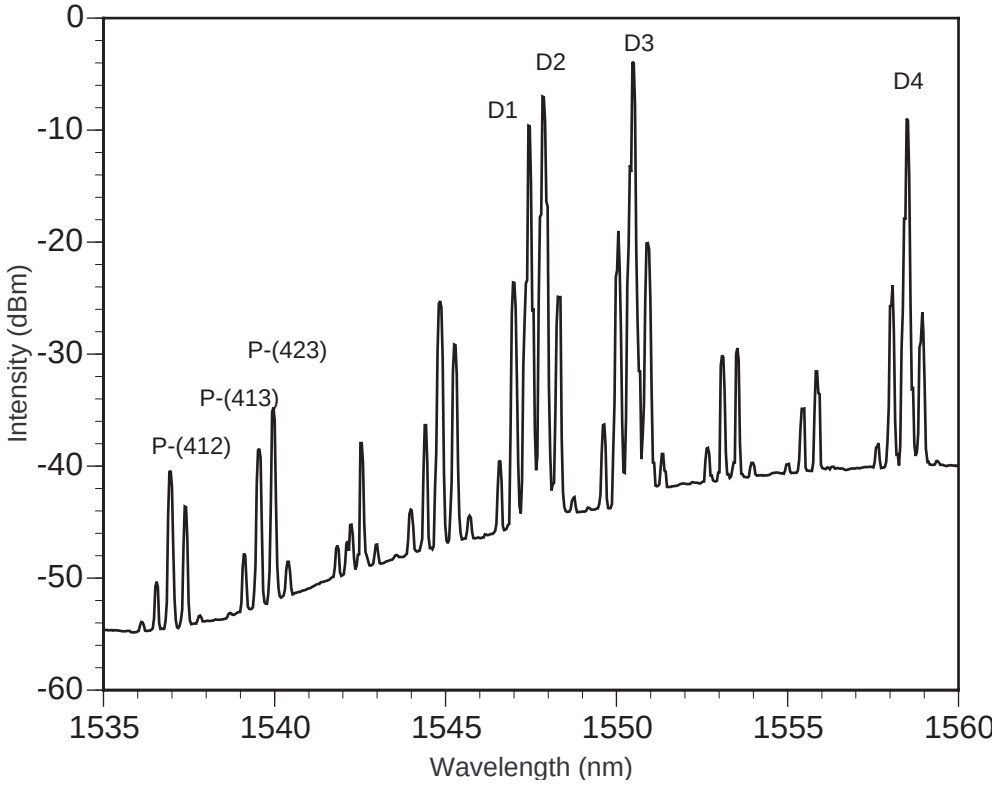

Figure 6.2: Optical Spectrum at the output of the SOA (in 0.1 nm Resolution Bandwidth) in the presence of four input waves (from Ref. [2])

In this case, the 3-bit adder circuit described above can be used as an encoder for the (7,4) Hamming Code, which simultaneously generates the three parity bits using different ND-FWM processes. Since D4 is common to all the additions, the pre-

processing element in one of the arms should act as a half-wave plate for D1, D2, and D3 and a full-wave plate for D4. The 7-bit word at the output of the encoder will be in a byte-wide format with the data and the parity bits on separate wavelength channels. Figure 6.2 shows the different FWM signals arising due to the presence of four wavelength channels [D1-D4] and the ND-FWM signals generating the parity bits are marked. Thus three independent logic functions can in principle be implemented in parallel in one circuit. This is schematically shown in Figure 6.3.

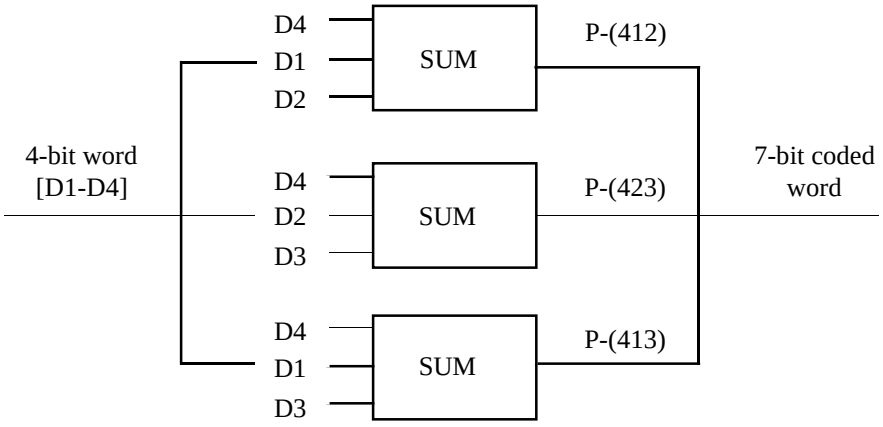

Figure 6.3: Generating the parity bits for the (7,4) Hamming Code

6.4 Decoder Circuit for the (7,4) Hamming Code

In a similar fashion, one way to realize a decoder circuit for the (7,4) Hamming code is by using the 3-bit adder circuits as building blocks and cascading them. The transmitted

code word contains the original four bits [D1-D4] and three parity bits [P-(412), P-(423), P-(413)]. To make a distinction between transmitted and received data, the transmitted bits are denoted by upper case while the received bits are denoted by lower case. Thus the transmitted word is [D1, D2, D3, D4, P-(412), P-(423), P-(413)], while the received word is [d1, d2, d3, d4, p-(412), p-(423), p-(413)]. For the sake of brevity, SUM[A1, A2, A3] and CARRY[A1, A2, A3] is used to denote the SUM and the CARRY bits resulting from the modulo-2 addition of the three bits A1, A2 and A3. Thus P-(412) = SUM[D4, D1, D2].

Since D4 is present in all three parity bits, it is the first bit that is checked for errors. The following additions are performed on the received bits,

$$d4\text{-}(12) = \text{SUM}[p\text{-}(412), d1, d2] \tag{6-7a}$$

$$d4\text{-}(23) = \text{SUM}[p\text{-}(423), d2, d3] \tag{6-7b}$$

$$d4\text{-}(13) = \text{SUM}[p\text{-}(413), d1, d3]. \tag{6-7c}$$

In the absence of any errors (received bit equals transmitted bit), each of the above additions would equal D4. For example, if d4-(12) is computed in the absence of any errors, it equals

$$\begin{aligned} d4\text{-}(12) &= \text{SUM}[p\text{-}(412), d1, d2] = \text{SUM}[P\text{-}(412), D1, D2] \\ &= (D4 \oplus \underline{D1 \oplus D2 \oplus D1 \oplus D2}) = D4, \end{aligned} \tag{6-8}$$

Since CARRY[A1,A2,A3] equals the bit that occurs the largest number of times among [A1-A3]. This can be used to find the correct transmitted bit D4 from the four bits [d4, d4-(12), d4-(23), d4-(13)] using the following operations,

$$D4 = \text{CARRY}[\text{CARRY}[d4, d4\text{-}(12), d4\text{-}(23)], \text{CARRY}[d4, d4\text{-}(23), d4\text{-}(13)], \text{CARRY}[d4, d4\text{-}(12), d4\text{-}(13)]]. \quad (6\text{-}9)$$

This ensures that D4 is correctly generated for all possible cases of the received code word including those with a single error on any bit. For example, if the error is on d2, i.e. $d2=\overline{D2}=D2 \oplus 1$,we obtain

$$d4\text{-}(12)=\text{SUM}[P\text{-}(412), D1, d2]=(D4 \oplus \underline{D1 \oplus D2 \oplus D1 \oplus D2} \oplus 1)=D4 \oplus 1=\overline{D4} \quad (6\text{-}10a)$$

$$d4\text{-}(23)=\text{SUM}[P\text{-}(423), D2, D3]=(D4 \oplus \underline{D2 \oplus D3 \oplus D2 \oplus D3} \oplus 1)=D4 \oplus 1=\overline{D4} \quad (6\text{-}10b)$$

$$d4\text{-}(13)=\text{SUM}[P\text{-}(413), D1, D3]= (D4 \oplus \underline{D1 \oplus D3 \oplus D1 \oplus D3}) = D4. \quad (6\text{-}10c)$$

In this case, the right-hand side of Equation (6-9) equals

$$\text{CARRY}[\text{CARRY}[D4, \overline{D4}, \overline{D4}], \text{CARRY}[D4, \overline{D4}, D4], \text{CARRY}[D4, \overline{D4}, D4]] = \text{CARRY}[\overline{D4}, D4, D4] = D4. \quad (6\text{-}11)$$

Similarly, if the error is on d4, i.e. d4= $\overline{D4}$=D4 ⊕ 1, the right-hand side of Equation (6-9) equals

$$\text{CARRY}[\text{CARRY}[\overline{D4}, \text{D4}, \text{D4}], \text{CARRY}[\overline{D4}, \text{D4}, \text{D4}], \text{CARRY}[\overline{D4}, \text{D4}, \text{D4}]]$$
$$= \text{CARRY}[\text{D4}, \text{D4}, \text{D4}] = \text{D4}, \qquad (6\text{-}12)$$

and if the error is on any one of the parity-bits, say p-(412),i.e., p-(412)=P-(412) ⊕ 1, the right hand side of Equation (6-9) equals

$$\text{CARRY}[\text{CARRY}[\text{D4}, \overline{D4}, \text{D4}], \text{CARRY}[\text{D4}, \text{D4}, \text{D4}], \text{CARRY}[\text{D4}, \overline{D4}, \text{D4}]]$$
$$= \text{CARRY}[\text{D4}, \text{D4}, \text{D4}] = \text{D4}. \qquad (6\text{-}13)$$

Figure 6.4 shows the block-diagram of a circuit that generates D4.

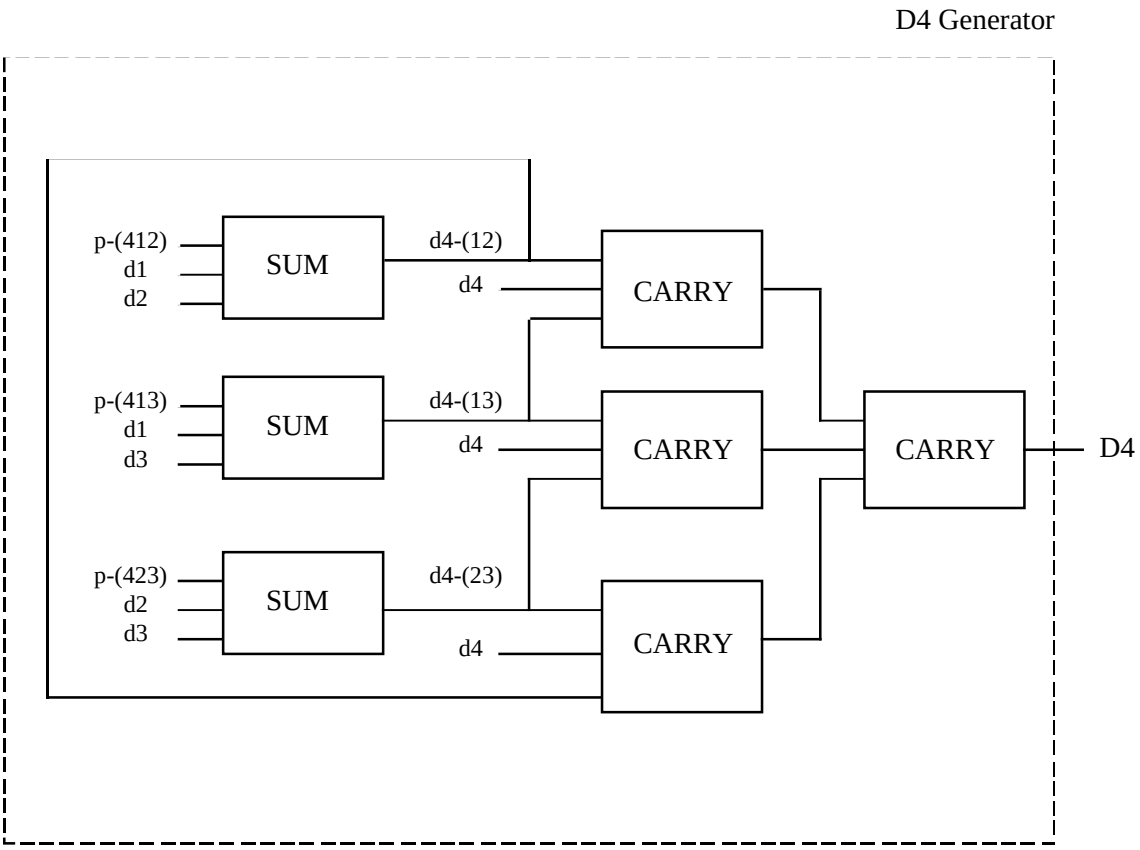

Figure 6.4: Generator circuit for D4

The other bits [D1-D3] occur symmetrically in the 7-bit word and can be found using the following additions:

$$d1\text{-}(42) = SUM[p\text{-}(412), d2, D4] \quad (6\text{-}14a)$$

$$d1\text{-}(43) = SUM[p\text{-}(413), d3, D4] \quad (6\text{-}14b)$$

$$D1 = CARRY[d1, d1\text{-}(42), d1\text{-}(43)] \quad (6\text{-}14c)$$

$$d2\text{-}(41) = SUM[p\text{-}(412), d1, D4] \quad (6\text{-}15a)$$

$$d2\text{-}(43) = SUM[p\text{-}(423), d3, D4] \quad (6\text{-}15b)$$

$$D2 = CARRY[d2, d2\text{-}(41), d2\text{-}(43)] \quad (6\text{-}15c)$$

$$d3\text{-}(41) = SUM[p\text{-}(413), d1, D4] \quad (6\text{-}16a)$$

$$d3\text{-}(42) = SUM[p\text{-}(423), d2, D4] \quad (6\text{-}16b)$$

$$D3 = CARRY[d3, d3\text{-}(41), d3\text{-}(42)]. \quad (6\text{-}16c)$$

It is easy to verify that the bits [D1-D3] are also generated correctly for all possible cases, where the received 7-bit word has at the most one erroneous bit. Figure 6.5 shows the block-diagrams of the circuits that generate the bits [D1-D3] once D4 has been generated.

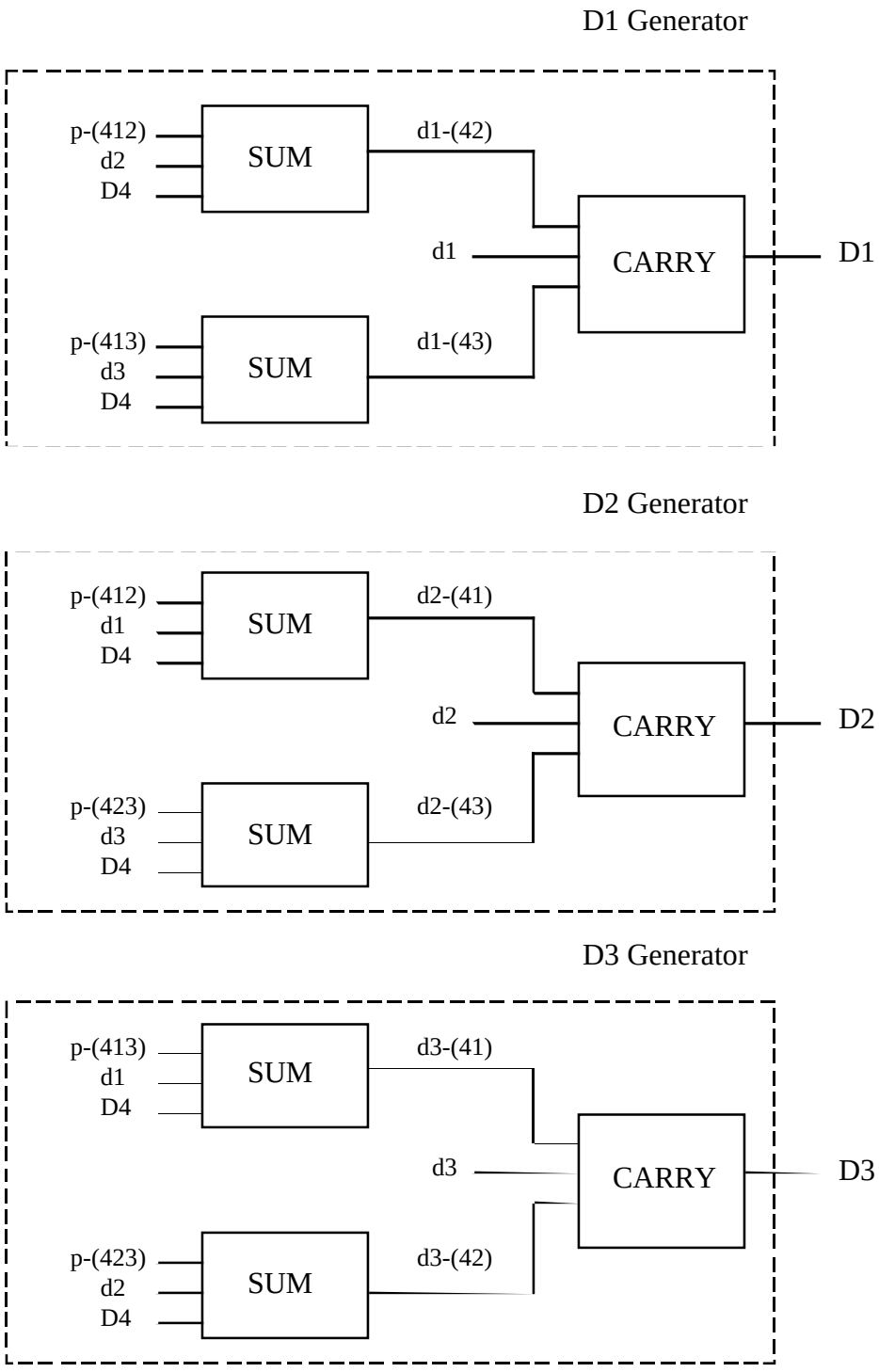

Figure 6.5: Generator circuits for bits [D1-D3]

6.5 Comments on Generalization

The experimental feasibility of cascading such circuits remains to be investigated. Issues such as the strength of the nonlinearity present in the devices used will determine the conversion efficiencies and Optical-Signal-to-Noise Ratios (OSNRs) of the FWM signals involved. The degradation of the Extinction Ratio (ER) of the PolSK signals due to mode conversion effects in these elements will affect the performance of these circuits and should be minimized. The results will be especially important in the design and implementation of more complex logic gates involving several Boolean operations, e.g., the decoding circuit for higher-level linear codes, such as the (7,4) Hamming Code.

The degradation of the ER of the PolSK bits can be modeled by using a Jones Matrix approach for each component (or cascades of several components). The ER of each component can be used to calculate an angular offset between the principal axes of the output with respect to the input of the component. The effect of this offset on the ER of the input PolSK bit can be calculated and the degraded ER of the PolSK bit can be obtained at the output. The procedure is repeated to find the ER as the PolSK bits pass through several components, each characterized by an ER.

Other Boolean functions can be realized by using cascaded FWM processes. One example is the parity-bit generation of the five bits [C1, C2, C3, C4, C5], which can be written as

$$P\text{-}(12345) = C1 \oplus C2 \oplus C3 \oplus C4 \oplus C5 = SUM[C1, C2, SUM[C3, C4, C5]]. \quad (6\text{-}17)$$

Thus, the 3-bit adder circuit also generates the parity-bit P-(12345) using two cascaded $\chi^{(3)}$ processes (or a fifth order nonlinear process). One way to implement the 5-bit parity generation is to choose the wavelengths for channels [C1-C5] such that the birefringent element (pre-processing element) acts as a wavelength selective half-wave plate for two channels, e.g., C1 and C4 and a full-wave plate for channels C2, C3, and C5. One of the four different cascaded scattering processes for the 5-bit parity generation is shown in Figure 6.6.

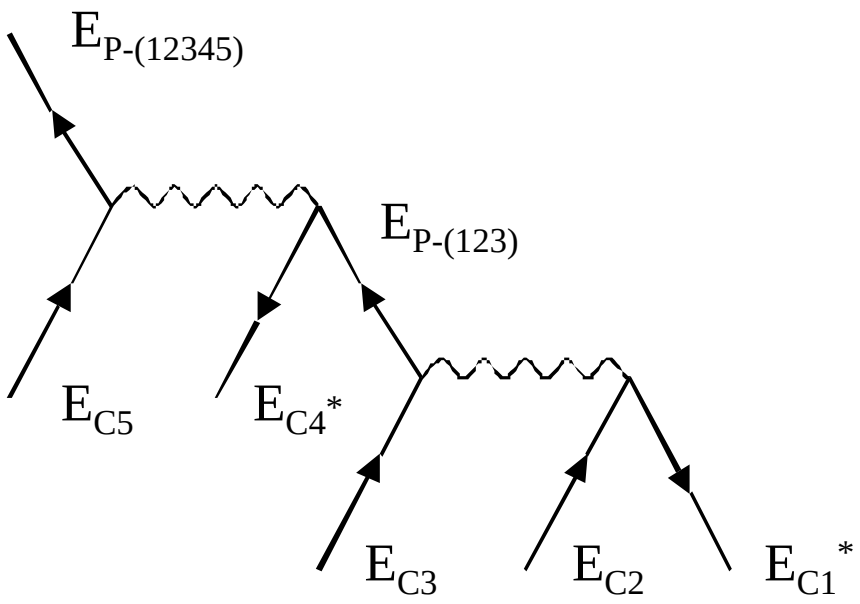

Figure 6.6: Two cascaded FWM processes can be used to implement a 5-bit parity generator

Depending on the strength of the nonlinearity in the device, the scheme can be generalized to the 7-bit parity generation using a seventh order nonlinear process and so on. In general, other types of building blocks for implementing other Forward Error-Correcting Codes (FECs) could be realized using different configurations and pre-processing elements. A comprehensive study of other types of logic elements is beyond the scope of this thesis.

6.6 Conclusion

It has been shown that FWM on PolSK coded bits can be used to construct certain higher-level logic elements without resorting to the standard 2-input gates. Taking the simple example of the (3,1) Hamming code, on-the-fly error correction on severely distorted data has been demonstrated. The data is recovered with a Bit Error Rate $<10^{-9}$. To the best of our knowledge, this is the first demonstration of a fiber optic logic circuit that performs signal processing on more than two input channels simultaneously. The bit rate of the experiment was limited to 2.5 Gbit/s by the bandwidth of the modulators. Since FWM is an ultrafast nonlinearity, the error correcting circuit can be made to perform at much higher bit rates. The scheme has been generalized, and it has been shown that a 3-bit adder can be implemented in a single circuit. It has also been shown that several ND-FWM processes can be used to perform different triple-product logic operations simultaneously and this can simplify the design of the encoder circuit for the (7,4) Hamming Code. Furthermore, the 3-bit adder circuit can be used as a building block to

implement more sophisticated Boolean functions, such as a decoder circuit for the (7,4) Hamming Code, without resorting to the standard 2-input transistor based logic using conventional electronic circuit theory. In passing, it should also be mentioned that the circuits designed for the (7,4) Hamming Code using the 3-bit adders reflect the symmetries of that error-correcting code. Finally, it should be noted that the error detection and correction schemes have been merely taken as examples to demonstrate the potential offered by using the polarization selection rules of ND-FWM processes to implement ultrafast all-optical logic.

Bibliography

1. V. Pless, "Introduction to the Theory of Error-Correcting Codes," John Wiley & Sons, New York, NY, 1982.

2. A. Bhardwaj, P.O. Hedekvist, and K. Vahala, "All-Optical Logic Circuits based on Polarization Properties of Nondegenerate Four-Wave Mixing," *J. Opt. Soc. Am. B*, **18**, 657-665 (2001).